JBC RESEARCH ARTICLE

Discovery of potent and selective PROTACs for the protein kinase LZK for the treatment of head and neck cancer

Received for publication, January 28, 2025, and in revised form, February 28, 2025 Published, Papers in Press, March 27, 2025,
https://doi.org/10.1016/j.jbc.2025.108452

Meghri Katerji[1,†], Knickole L. Bergman[1,†], Eric Lindberg[2,‡], Maxine R. Rubin[1,‡], Marwa Afifi[3], Amy L. Funk[1], Carolyn C. Woodroofe[2], Katherine Nyswaner[1], Kamila Karpińska[4], Remigiusz Serwa[5], Steven D. Cappell[3], Anna Marusiak[4], Rolf E. Swenson[2,*], and John F. Brognard[1,*]

From the [1]Laboratory of Cell and Developmental Signaling, Center for Cancer Research, National Cancer Institute at Frederick, National Institutes of Health, Frederick, Maryland, USA; [2]Chemistry and Synthesis Center, National Heart, Lung, and Blood Institute, National Institutes of Health, Rockville, Maryland, USA; [3]Laboratory of Cancer Genetics and Cell Biology, Center for Cancer Research, National Cancer Institute, Bethesda, Maryland, USA; [4]Laboratory of Molecular OncoSignalling, IMol Polish Academy of Sciences, Warsaw, Poland; [5]Proteomic Core Facility, IMol Polish Academy of Sciences, Warsaw, Poland

Reviewed by members of the JBC Editorial Board. Edited by Paul Shapiro

Leucine zipper–bearing kinase (LZK) is overexpressed in 20% of head and neck squamous cell carcinoma (HNSCC) cases and has emerged as a promising therapeutic target in this cancer subtype. LZK promotes HNSCC survival and proliferation by stabilizing c-MYC and GOF-p53 in kinase-dependent and -independent manners, respectively. Herein, we developed a new series of LZK degraders utilizing proteolysis-targeting chimera (PROTAC) technology by modulating the linker region or LZK warhead of LZK-targeting PROTAC-21A, previously developed by our laboratory. Among the 27 PROTACs synthesized and tested, PROTAC 17 was found to be the most potent, degrading LZK at 250 nM and suppressing HNSCC viability at 500 nM. In summary, our lead PROTAC effectively targeted LZK for proteasomal degradation and inhibited oncogenic activity in HNSCC cell lines with amplified LZK.

Leucine zipper–bearing kinase (LZK), encoded by *MAP3K13*, is a serine/threonine protein kinase belonging to the mixed lineage kinase family (1). Compared with many mitogen-activated protein kinase kinase kinases, LZK is self-activated upon overexpression, *via* leucine zipper–mediated homomeric interaction and autophosphorylation of the kinase domain. This self-activating property is consistent with the low expression of endogenous LZK protein under normal conditions (1–3), whereas in cancer, amplification leads to activation of this kinase. LZK regulates signaling pathways including the mitogen-activated protein kinase cascade leading to c-Jun N-terminal kinase (JNK) activation and is involved in various biological processes, including cellular response to stress, apoptosis, and cell differentiation (3, 4). LZK has been implicated in several pathological diseases, such as neurodegenerative diseases, inflammation, and cancer, and is considered a promising target for therapeutic intervention (5–7).

Recent work from our group established LZK as an oncogenic driver in head and neck squamous cell carcinoma (HNSCC) (6). Approximately 20% of HNSCC cases are characterized by amplification of *MAP3K13* with an additional 50% presenting with gains of this kinase (8), indicating that approximately 70% of HNSCC patients rely on this oncogenic kinase to maintain cancer cell proliferation. Our laboratory identified amplified *MAP3K13* as a novel genetic dependency in HNSCC through knockdown experiments and explored the potential of LZK to serve as a favorable therapeutic target in this cancer subtype using small-molecule inhibitors (6, 9). In the study by Funk *et al.* (9), we also discovered that LZK promotes proliferation of HNSCC by maintaining expression of c-MYC and GOF-p53 in kinase-dependent and -independent manners, respectively. To abolish both catalytic and noncatalytic oncogenic functions of LZK, we developed a proteolysis-targeting chimera (PROTAC) that specifically promotes LZK degradation, leading to reduced expression of c-MYC and GOF-p53 as well as inhibition of cell cycle progression. PROTACs are heterobifunctional molecules consisting of three main parts: a protein of interest (POI) ligand, an E3 ubiquitin ligase–recruiting ligand, and a linker connecting these two ligands (10). Degradation of the POI occurs when a ternary complex is formed between the POI and E3 ligase. This allows for the POI to be ubiquitinated and recognized by the 26S proteasome for degradation (10, 11).

Here, we describe the generation of 27 novel LZK-targeting PROTACs, with the goal of improving the efficacy and potency of the first-generation PROTAC-21A. The novel LZK-targeting PROTACs showed early promise in their abilities to degrade LZK and inhibit downstream signaling as well as reduce cell proliferation and survival of HNSCC cells with amplified LZK at nanomolar concentrations, with compound **17** outperforming our first-generation lead PROTAC, PROTAC-21A. Importantly, our study continues to demonstrate the promise of targeting LZK as a potential new treatment strategy for HNSCC patients with the use of PROTACs.

† Denotes co-first authors.
‡ These authors contributed equally to this work.
* For correspondence: Rolf E. Swenson, rolf.swenson@nih.gov; John F. Brognard, john.brognard@nih.gov.

Results

To target both catalytic and noncatalytic oncogenic functions of LZK, our laboratory has previously developed PROTAC-21A, based on the LZK inhibitor acylated compound **21** (structure in abstract) (12) and Von Hippel–Lindau VHL1 E3 ubiquitin ligase binder (9, 13). This compound was shown to completely degrade LZK and significantly reduce clonogenic growth at 1 μM (9) as well as inhibit cell cycle progression (Fig. S1), comparable to depletion of LZK (6). In this study, we generated 23 new LZK-targeting PROTACs by modulating the linker region of PROTAC-21A with the goal of improving its potency. We evaluated the efficacy of these synthesized PROTACs for their ability to degrade LZK and inhibit downstream JNK signaling in CAL33 cell line with doxycycline (dox)-induced LZK overexpression. LZK is a mitogen-activated protein kinase kinase kinase that activates the JNK pathway by directly phosphorylating MAP2Ks, MKK4, and MKK7 (14). Exogenously overexpressed LZK leads to JNK pathway activation, making this a useful readout to assess LZK degradation and inhibition of the JNK pathway because of PROTAC-mediated degradation of LZK (9). To determine an optimal linker for achieving better LZK degradation, CAL33 LZK-expressing cells were treated with different concentrations of these compounds, ranging from 0.1 to 10 μM for 24 h. Our novel LZK-targeting PROTACs had varying levels of potency. While some of these compounds (**1**–**9**) (Fig. 1) did not have prominent effects in degrading LZK (Fig. 2), compounds **10** to **21** (Fig. 3) performed at least similarly if not better than PROTAC-21A (Fig. 4). From this compound collection, we identified PROTAC **17** as the most efficacious, causing LZK degradation at 250 nM, followed by PROTAC **16** and **21** with degradation of LZK observed at 500 nM. The linker used in compound **21** is the shortest one tested, composed of only one carbon, and compound **17** has one of the most rigid linkers because of the angles of the cyclobutane. These data suggest that making the linker region short and rigid can make it more thermodynamically favorable for the E3 ligase to ubiquitinate LZK.

We also generated LZK-targeting PROTACs using different versions of E3 ligase ligand, such as MDM2 in compound **22**, and VHL2 in compound **23**, as well as modified LZK ligands such as cyanopyridine to pyrazine modification of acylated compound **21** in compound **24** and **25**, and a scaffold hop to a pyrazole core in compounds **26** and **27** (as described in Ref. (15)) (Fig. S2). However, none of these PROTACs were found to be potent in degrading LZK in LZK-expressing CAL33 cells (Fig. S3). Interestingly, compounds **24** and **25** are identical to compound **17** and PROTAC-21A except for the modification in the acylated compound **21** LZK warhead; however, their efficacy was reduced because of this alteration with LZK degradation dropping to 1 μM instead of 250 nM and 500 nM, respectively, indicating the importance of cyanopyridine for the LZK-binding ligand.

Of the 27 PROTACs developed and tested, compound **17** was taken forward to be evaluated further for its potent LZK-degrading capability and specificity. The thermodynamic interaction affinity of the lead compound **17** toward LZK (K_d = 71 nM) was determined to be comparable to that of PROTAC-21A (previously reported as K_d = 35 nM) (9) using an ATP-independent competition binding assay (Fig. 5*A*). We examined the time-course effect of PROTAC **17** in degrading LZK and showed degradation as early as 1 h for up to 24 h, with LZK signal reappearing at 48 h (Fig. 5*B*). Interestingly, pJNK signal rebounded at 24 h despite loss of LZK expression, indicating a stress response mechanism activated by PROTAC **17**, consistent with the discrepancy observed between LZK expression and JNK phosphorylation in the dose–curve Western blot analysis for PROTAC 17 (Fig. 4). We verified that the reduction of LZK abundance by PROTAC **17** is due to proteasomal-mediated degradation, as LZK degradation by the PROTAC was prevented by treatment of cells with proteasome inhibitor MG-132 and neddylation inhibitor MLN4924 (Fig. 5*C*). We then compared the potency of PROTAC **17** to the first-generation PROTAC-21A in HNSCC cell lines using long-term colony-formation assay. PROTAC-21A was previously reported to cause 75% reduction of colony-forming ability of amplicon-positive cells at 1 μM (9), without having significant effects at 500 nM (Fig. S4*A*). PROTAC **17** caused almost complete loss of colony-forming ability of two HNSCC cell lines harboring amplified *MAP3K13* (CAL33 and DETROIT562) at a lower concentration of 500 nM, and only minor effects were observed in BICR22 HNSCC control cell line lacking amplified *MAP3K13* (Fig. 5, *D* and *E*). At lower concentration of 250 nM, PROTAC **17** also reduced colony formation of CAL33 and DETROIT562 to a similar extent as 1 μM of PROTAC-21A, without having any effect on BICR22 (Fig. S4*B*).

We validated the specificity of PROTAC **17** using a mass spectrometry (MS)–based global proteomic analysis in CAL33 cells upon dox-induced LZK expression (Fig. 6*A*) followed by treatment with a dimethyl sulfoxide (DMSO) control or 500 nM PROTAC **17** (Fig. 6*B*). The results confirmed significant overexpression of LZK after dox induction, and a downregulation of LZK protein after PROTAC **17** treatment, with the relative expression change being the highest for LZK protein (File S1). To further confirm the specificity of our lead PROTAC, we also developed a control compound for compound **17** with a 1,3-*cis*-cyclobutane linker, preventing VHL ligase recruitment because of stereospecificity of VHL, and as predicted, the *cis*-epimer of PROTAC **17** (Fig. 6*C*) did not degrade LZK up to 2.5 μM (Fig. 6*D*) and had no effect on the colony-forming ability of HNSCC cells at the concentrations tested (Figs. S4*C*, 6*B*).

Finally, pharmacodynamic properties also play a key role in the success of developing a potent PROTAC. We examined the permeability property of our novel LZK-targeting PROTACs across an artificial membrane using a parallel artificial membrane permeability assay (PAMPA) (Cyprotex). The mean permeabilities of our compounds were low compared with the high and low permeability controls, likely because of their

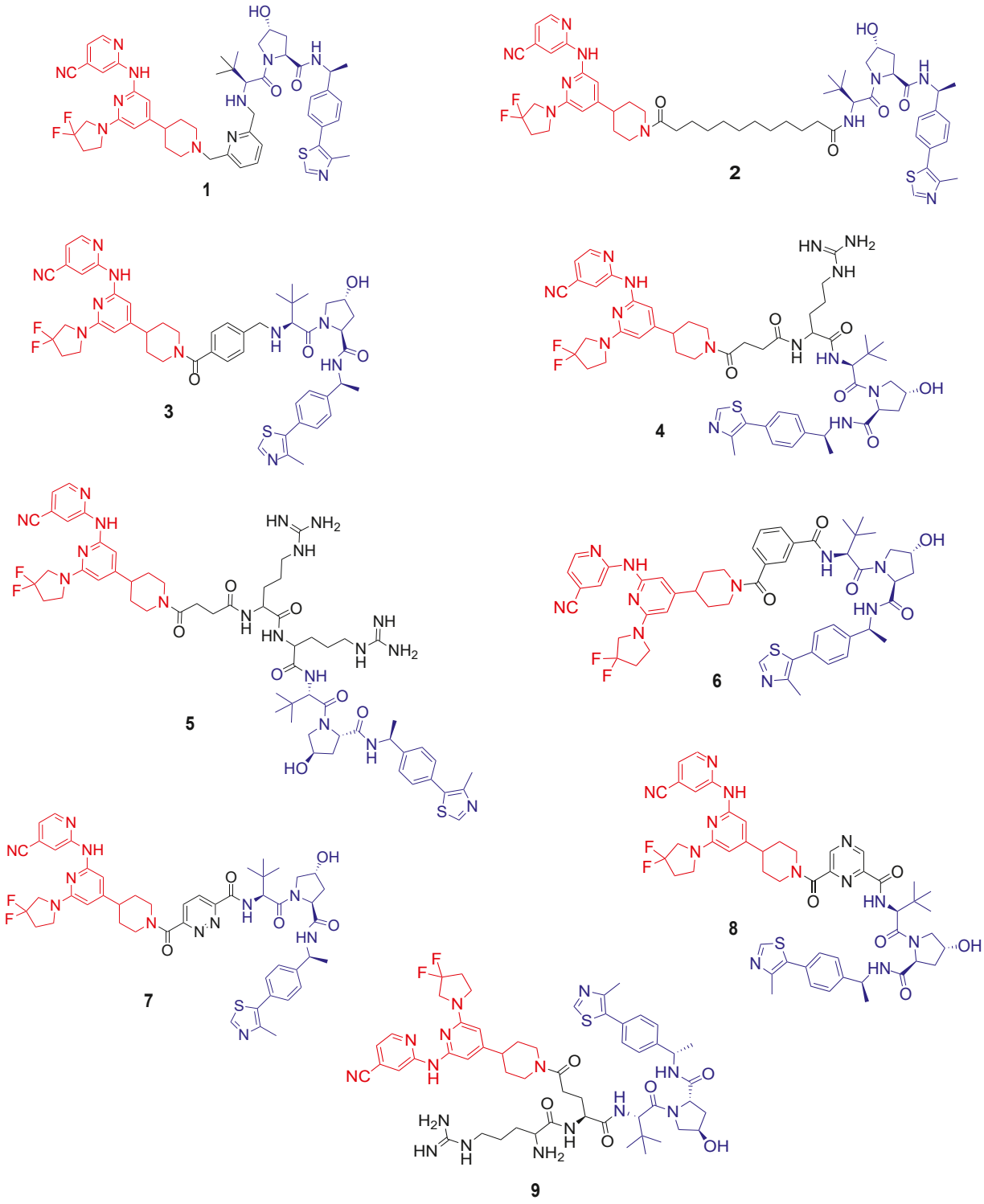

Figure 1. Chemical structures of LZK-targeting PROTACs 1 to 9. All PROTACs have the same LZK-targeting warhead (acylated compound 21—in *red*) and E3 ligase–recruiting ligand (VHL ligand—in *blue*). The linker region depicted in *black* is altered from the first-generation LZK-targeting PROTAC-21A in these different compounds. LZK, leucine zipper–bearing kinase; PROTAC, proteolysis-targeting chimera.

large molecular weight, with most of the values ranging from -0.0028×10^{-6} to 0.0100×10^{-6} cm/s, except for compound **6** and **8**, which had PAMPA scores of 8.84 and 12.59×10^{-6} cm/s (Table 1).

Discussion

HNSCC is the sixth most common cancer with limited treatment options (16). Reduction of LZK activity or abundance suppresses HNSCC cell proliferation and survival. Thus,

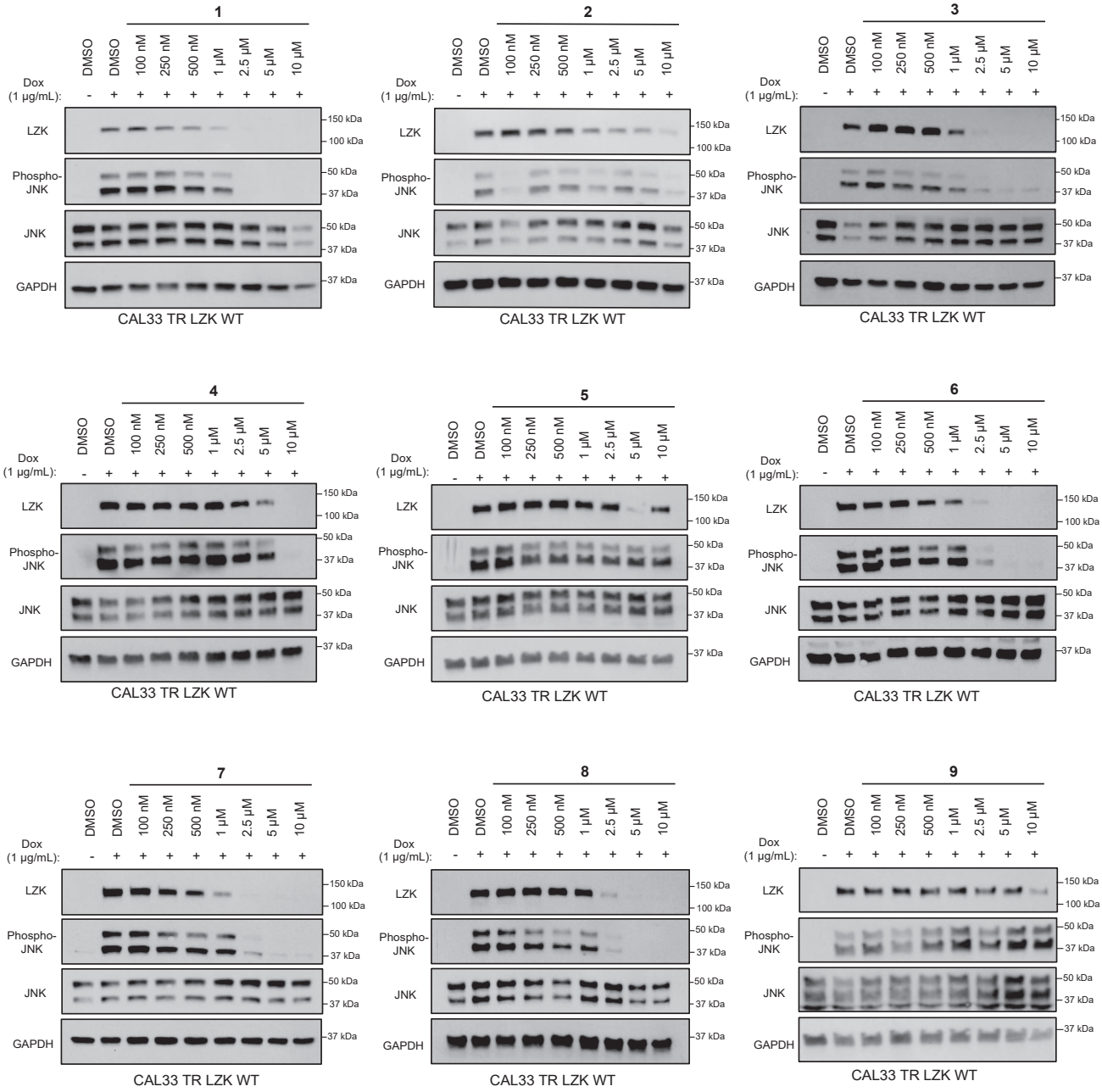

Figure 2. Western blot analysis showing the effect of increasing concentrations of PROTACs 1 to 9 treated for 24 h on LZK expression and JNK phosphorylation in response to doxycycline (dox)-induced expression of LZK in CAL33 cells. GAPDH served as the loading control. JNK, c-Jun N-terminal kinase; LZK, leucine zipper–bearing kinase; PROTAC, proteolysis-targeting chimera.

LZK-targeting PROTACs show early promise in their ability to be used as a novel treatment option for HNSCC patients harboring amplified *MAP3K13*.

The key factors for the success of a PROTAC include the warhead's strong and selective binding to the target, efficient recruitment of the E3 ubiquitin ligase, and formation of a stable ternary complex, as well as favorable pharmacodynamic characteristics. Here, we work toward optimizing the structure of LZK-targeting PROTAC by altering the linker region or LZK warhead to improve the potency of our previously developed LZK degrader, PROTAC-21A. Of 27 novel LZK-targeting PROTACs, which had varying levels of LZK degradation, inhibition of downstream activity, and permeability across the membrane, PROTAC **17** was identified as a potent lead compound outperforming the first-generation PROTAC-21A by selectively inducing a dose- and time-dependent degradation of LZK in HNSCC cells harboring *MAP3K13* amplification. However, this study also revealed some of the shortcomings of the generated LZK-targeting PROTACs. In particular, low pharmacodynamic properties particularly need to be optimized in the future so we can continue to work toward investigating their effects in suppressing HNSCC tumor growth *in vivo* and establishing a novel therapeutic strategy for HNSCC patients. In future studies, we aim to improve formulation to ensure we

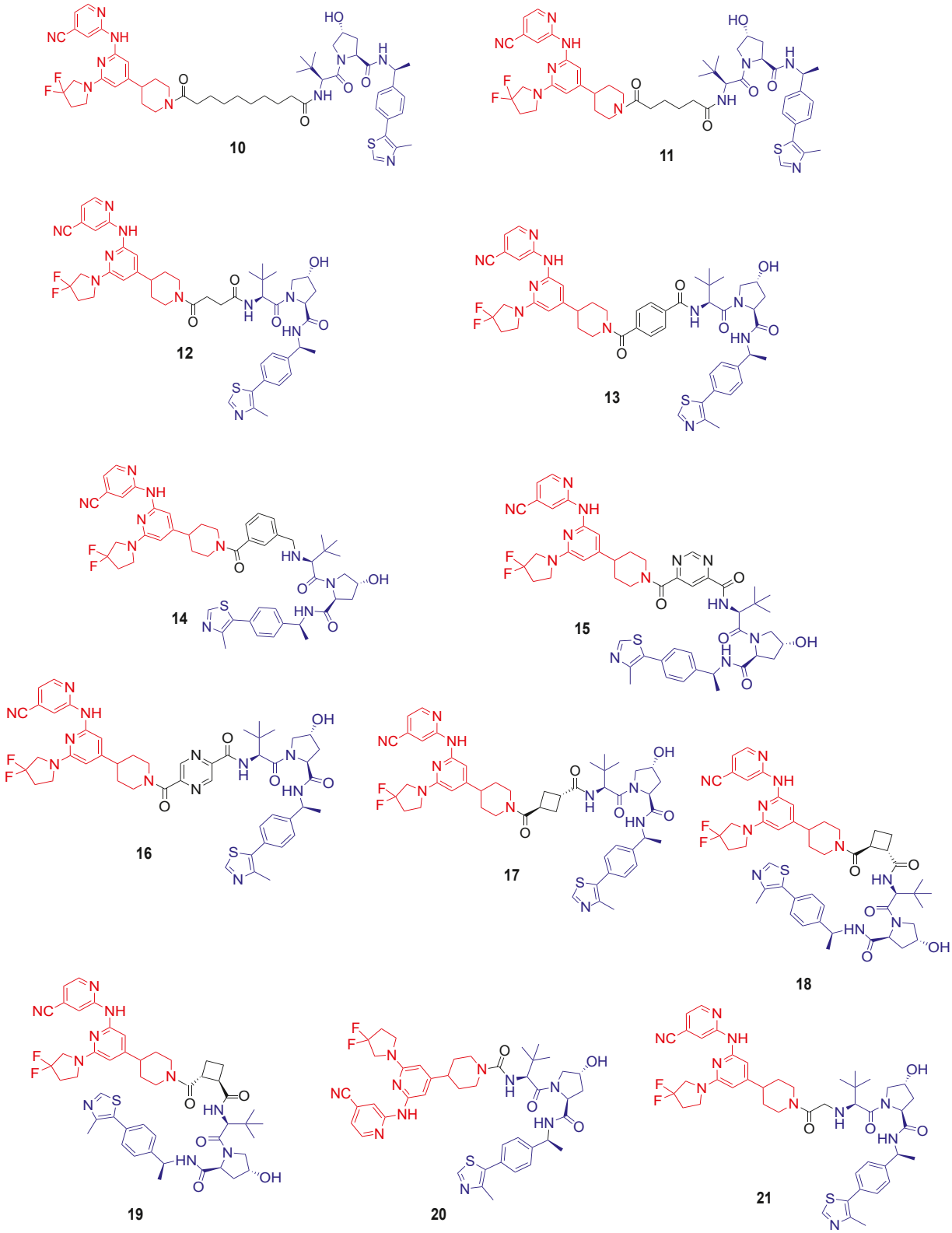

Figure 3. Chemical structures of LZK-targeting PROTACs 10 to 21. All PROTACs have the same LZK-targeting warhead (acylated compound 21—in *red*) and E3 ligase–recruiting ligand (VHL ligand—in *blue*). The linker region depicted in *black* is altered from the first-generation LZK-targeting PROTAC-21A in these different compounds. LZK, leucine zipper–bearing kinase; PROTAC, proteolysis-targeting chimera.

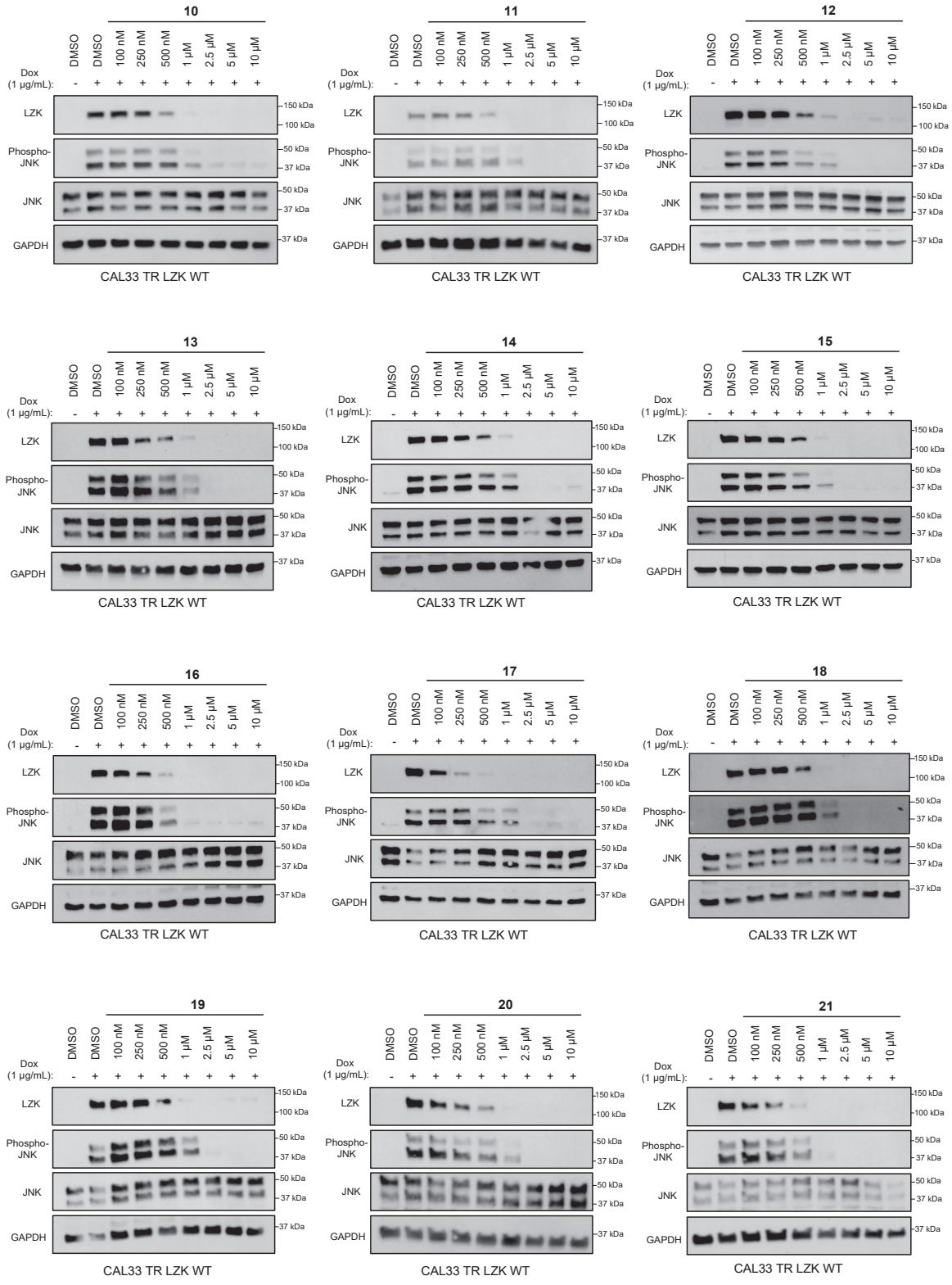

Figure 4. Western blot analysis showing the effect of increasing concentrations of PROTACs 10 to 21 treated for 24 h on LZK expression and JNK phosphorylation in response to doxycycline (dox)-induced expression of LZK in CAL33 cells. GAPDH served as the loading control. JNK, c-Jun N-terminal kinase; LZK, leucine zipper–bearing kinase; PROTAC, proteolysis-targeting chimera.

can achieve optimal delivery of our lead PROTAC to tumors with increased half-life and bioavailability. In addition, we will also utilize improved inhibitors we have developed in the laboratory that are more potent and have improved pharmacokinetic properties as the LZK binder and building on our linkers presented here with the overall goal of developing a clinical development candidate for preclinical and toxicology studies. Overall, the data presented here will guide the

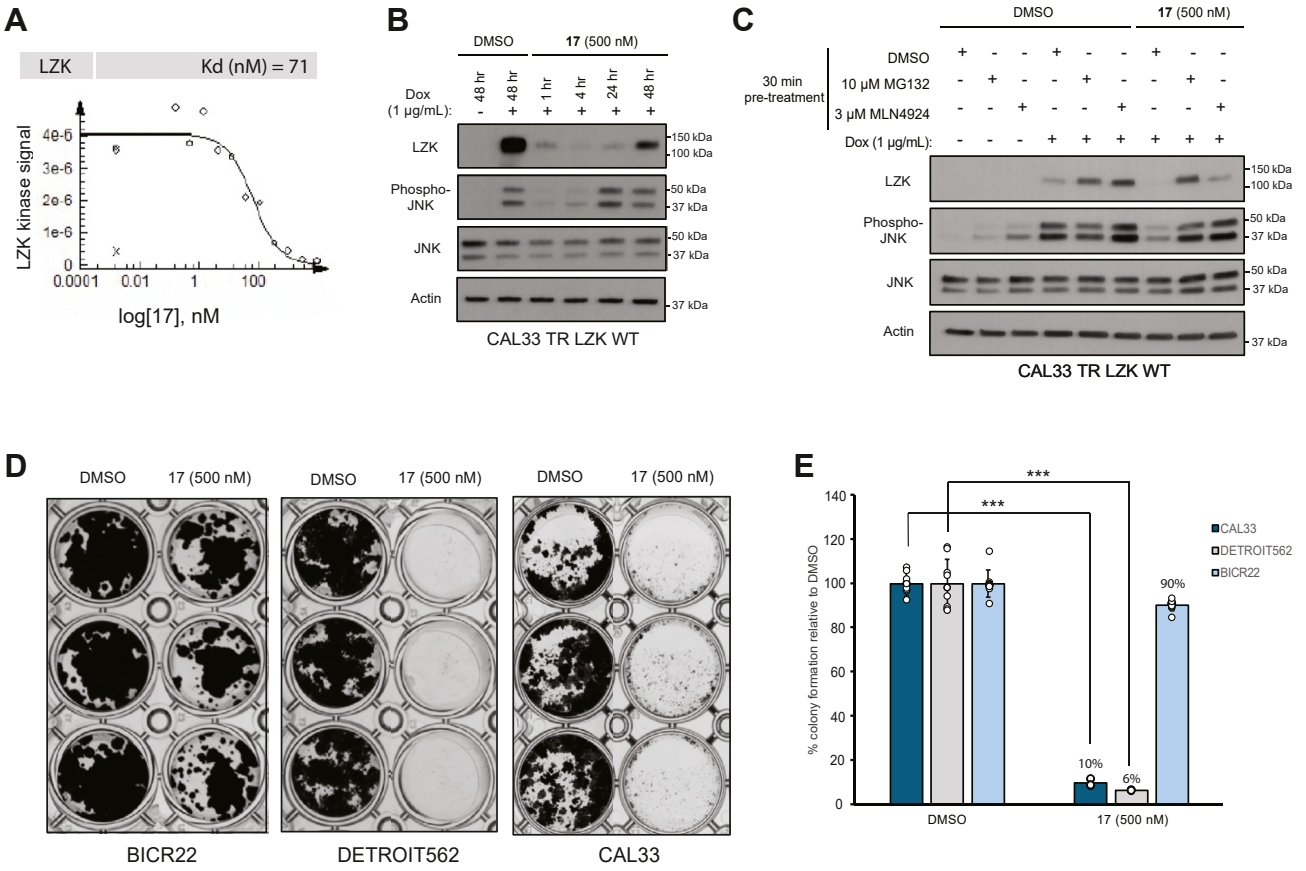

Figure 5. Evaluation of LZK-targeting PROTAC 17 proteasome-mediated degradation ability and its effects on HNSCC cell growth. *A*, dose curve of the *in vitro* binding affinity of PROTAC 17 to LZK, assessed by Eurofin's KdELECT KINOMEscan profiling. The amount of kinase measured by quantitative PCR (signal; *y*-axis) is plotted against PROTAC 17 concentration in nanometer in log10 scale (*x*-axis). *B*, Western blot analysis showing time-course effect of PROTAC 17 on LZK expression and JNK phosphorylation in response to dox-induced LZK WT expression in CAL33 cells. GAPDH served as the loading control. *C*, Western blot showing dependence of PROTAC17-mediated degradation of LZK involves both ubiquitin-like molecule NEDD8 and the proteasome. LZK was induced with dox in CAL33 cells, and the cells were pretreated for 30 min with either MG132 to inhibit the proteasome or MLN4924 to inhibit NEDD8 and then exposed to the indicated concentration of PROTAC 17 for 8 h. Expression level of LZK was monitored. GAPDH served as the loading control. *D* and *E*, effect of PROTAC 17 on colony formation by indicated HNSCC cell lines. DMSO served as the vehicle control. Cells were treated for 14 days with the drug being replaced every 48 h. Plates were fixed and stained with crystal *violet* and visualized. Crystal *violet* stain was solubilized with acetic acid and measured at 595 nm. Individual data points represent technical replicates of one experiment. Data are representative of three independent experiments. Significant differences were determined by Student's *t* test (***$p < 0.001$). DMSO, dimethyl sulfoxide; dox, doxycycline; HNSCC, head and neck squamous cell carcinoma; JNK, c-Jun N-terminal kinase; LZK, leucine zipper–bearing kinase; PROTAC, proteolysis-targeting chimera.

optimization and development of LZK-targeting PROTACs, enhancing their potency against HNSCC. Finally, our work has a broader implication as the collection of PROTACs generated by altering the linker region could also serve as an invaluable tool for the research community to optimize PROTAC structures for other protein targets.

Experimental procedures

Cell culture

CAL33 cells (DSMZ) and SCC15 cells (American Type Culture Collection) were maintained in Dulbecco's modified Eagle's medium (Sigma–Aldrich) supplemented with 10% fetal bovine serum (FBS) (Atlanta Biologicals), 1% penicillin–streptomycin (pen–strep; Gibco), and 2 mmol/l GlutaMAX (Gibco). BICR22 cells (Sigma) were grown in Dulbecco's modified Eagle's medium (Sigma–Aldrich) with 10% FBS, 1% pen–strep, 0.4 μg/ml hydrocortisone (Sigma), and 2 mmol/l GlutaMAX. DETROIT562 cells (American Type Culture Collection) were maintained in Eagle's minimal essential medium with 10% FBS, 1% pen–strep, and 2 mmol/l GlutaMAX. All cells were incubated at 37°C and 5% CO_2. All cell lines were verified by Short Tandem Repeat profiling. Cell lines were used in experiments for fewer than 20 passages (10 weeks) after thawing. A Visual-PCR Mycoplasma Detection Kit (GM Biosciences) was used to confirm cell lines in use were mycoplasma negative.

Generation of tetracycline-inducible expression cell line

To generate CAL33 cells with tetracycline-inducible expression of LZK WT, the ViraPower HiPerform T-Rex Gateway Expression System (Invitrogen) was used. Briefly, human embryonic kidney-293T cells were transfected with LZK (cloned into pLenti6.3/TO/V5-DEST vector) and pLenti3.3TR (for tetracycline repressor expression) using Lipofectamine 2000 to generate lentiviral stocks. CAL33 cells were then transduced with lentiviral stocks, and cells were generated by antibiotic selection with blasticidin (Invitrogen)

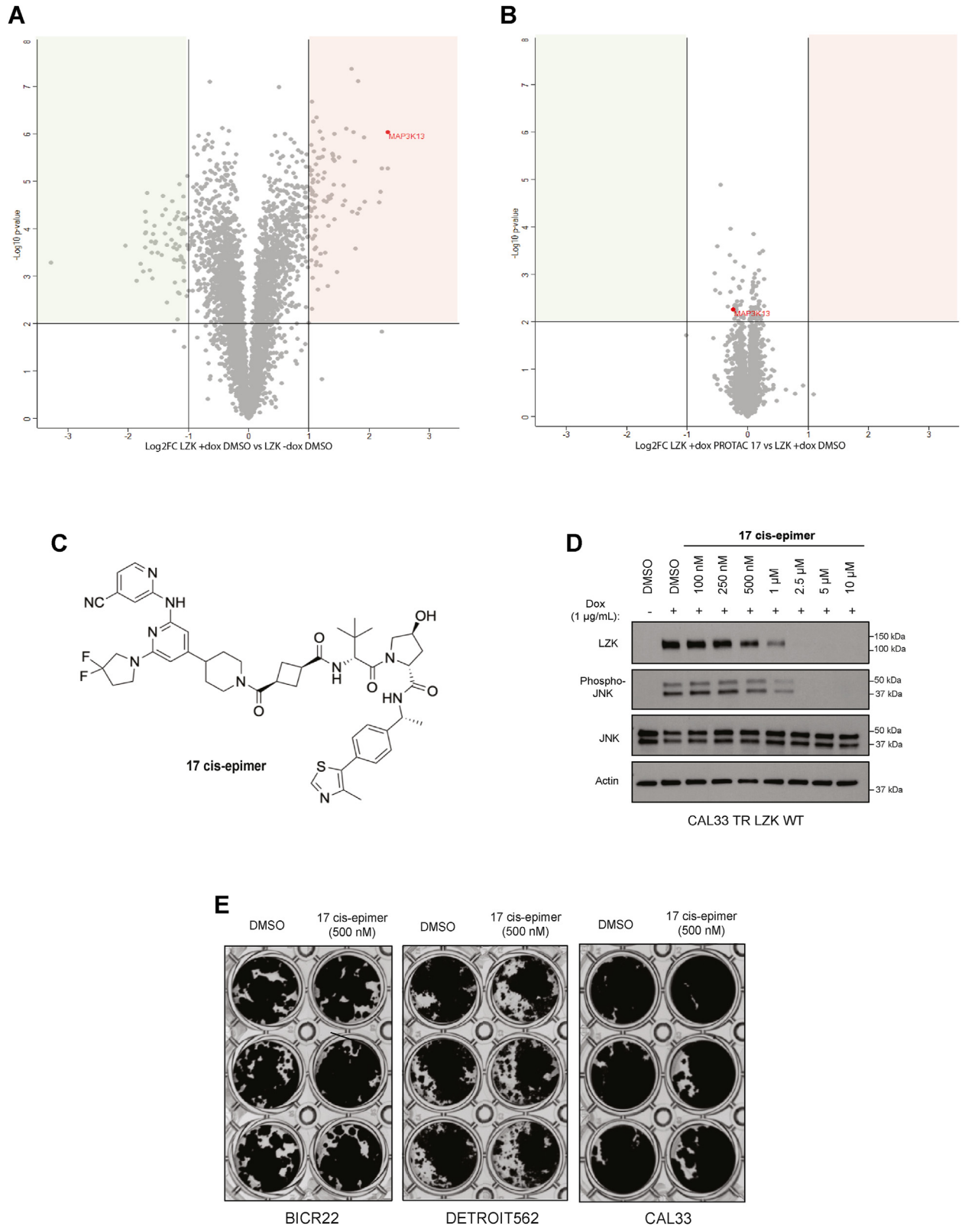

Figure 6. Specificity of PROTAC 17 toward LZK. *A* and *B*, shotgun proteomic analysis of total cell protein extracts from CAL33 TR LZK WT cell line following treatment with PROTAC 17. CAL33 TR LZK WT cells were treated with doxycyline (dox) to induce LZK overexpression, followed by treatment with 500 nM PROTAC 17 or DMSO control for 24 h. LZK protein is indicated in *red*. Volcano plot displaying the Log2 fold change (Log2FC, *x*-axis) against the *t* test-derived −log10 statistical (n = 3) *p* value (*y*-axis) for all proteins detected in the total cell extract from CAL33 TR LZK WT cells after dox induction of LZK overexpression. The change thresholds of Log2FC ≥|1.0| and the significance threshold of −log10 *p* value ≥2.0 were applied to identify proteins with levels decreased (*green boxed area*) or increased (*red boxed area*) in response to the dox treatment (*A*). Volcano plot displaying the Log2FC (*x*-axis) against the *t*-test-derived −log10 statistical (n = 3) *p* value (*y*-axis) for all proteins detected in the total cell extract from CAL33 TR LZK WT cells following induction of LZK overexpression and the treatment with PROTAC 17 or DMSO. The change thresholds of Log2FC ≥|1.0| and the significance threshold of −log10 *p* value

Table 1
PAMPA assay for VHL-based LZK-targeting PROTACs developed in this study

Compound	PAMPA mean permeability ($x10^{-6}$ cm/s)
1	−0.0007
2	<0.01
3	0.0019
4	—
5	—
6	8.84
7	−0.0002
8	12.59
9	0.01
10	<0.01
11	0.0009
12	−0.0008
13	−0.0002
14	7.4
15	0
16	0.0006
17	0.01
18	0.0006
19	0.0022
20	0
21	−0.0028

and geneticin (Gibco). Tetracycline (1 μg/ml; Invitrogen) was used to induce expression of LZK.

PROTAC/inhibitor treatment

All PROTACs were developed in-house. MG132 was purchased from Selleck Chemicals. MLN4924 was purchased from MedChemExpress. All compounds were dissolved in DMSO, and DMSO was used as the vehicle control in the cell-based assays.

Chemical synthesis

Reagents were purchased from commercial sources and used without further purification. *tert*-Butyl4-(2-chloro-6-(3,3-difluoropyrrolidin-1-yl)pyridin-4-yl)piperidine-1-carboxylate and 6-(3,3-difluoropyrrolidin-1-yl)-4-(piperidin-4-yl)-*N*-(4-(trifluoromethyl)pyridin-2-yl)pyridin-2-amine were prepared as previously described (12). Final products were purified by flash chromatography or preparative HPLC. All tested compounds were characterized by LC–MS. NMR spectra were obtained on a 400 MHz Varian and 500 MHz Bruker NMR and processed using MestreNova software (Mestralab). LC–MS data for small molecules were acquired on an Agilent Technologies 1290 Infinity HPLC system using a 6130 quadrupole LC–MS detector and a Poroshell 120 SB-C18 2.7 μm column (4.6 × 50 mm) or an Agilent 1200 series HPLC system with an LC/MSC Trap XCT detector and a ZORBAX 300SB-C18 3.5 μm column (4.6 × 50 mm). Preparative HPLC chromatography was performed on a Shimadzu system using a 30 mm × 150 mm Xbridge C18 column (Waters). Flash chromatography was performed on a Teledyne ISCO CombiFlash Rf+. High-resolution mass spectrometry (HRMS) data were acquired on a Waters Xevo G2-XS QTof running MassLynx version 4.1.

General method 1A

To a solution of 2-((6-(3,3-difluoropyrrolidin-1-yl)-4-(piperidin-4-yl)pyridin-2-yl)amino)isonicotinonitrile dioxalate salt (1 eq) in dry dimethylformamide (DMF) (1 ml) was added *N*-methylmorpholine (NMM; 5 eq), and the solution was stirred under argon for 5 min. To a solution of *bis*-acid (2 eq) in dry DMF (1 ml) was added O-(7-azabenzotriazol-1-yl)-*N*,*N*,*N*′,*N*′-tetramethyluronium hexafluorophosphate (HATU) (1.3 eq) and NMM (2 eq), and the solution was stirred for 5 min. The activated acid was added to the DMF solution containing the LZK inhibitor. The reaction was monitored by LC–MS until the reaction was complete (0.5–1 h), and water was added to the reaction mixture and stirred for 30 min. The reaction solution was extracted with dichloromethane (DCM) three times. The combined organic layer was washed with saturated sodium bicarbonate solution, brine, dried over sodium sulfate, filtered, and concentrated under reduced pressure. The crude LZK-inhibitor acid product was used in the next step without further purification.

General method 1B

To a solution of the LZK-acid (1 eq) in DMF (1 ml) was added (2S,4R)-1-((S)-2-amino-3,3-dimethylbutanoyl)-4-hydroxy-*N*-((S)-1-20 (4-(4-methylthiazol-5-yl)phenyl)ethyl) pyrrolidine-2-carboxamide hydrochloride (1 eq) and NMM (4 eq), and the solution was stirred under argon for 5 min. HATU was added (1 eq), and the reaction was stirred at room temperature for 30 min after which water was added, and the mixture was stirred for 20 min. The solution was then extracted with DCM and washed with saturated sodium bicarbonate and brine. The organic layer was then dried over sodium sulfate, filtered, and concentrated *in vacuo*. The crude residue was purified by flash chromatography using gradient elution (0–10% methanol in DCM) over 20 column volumes in a 4 g silica column. The compound was further purified by reverse-phase HPLC (RP-HPLC) using a Waters XBridge Prep Cl8 5 μm 19 mm × 150 mm column in water (0.05% TFA) with an increasing gradient of acetonitrile (0.05% TFA). The combined fractions were lyophilized to afford the product as a yellow solid.

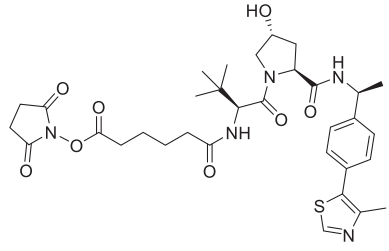

≥2.0 were applied to identify proteins with levels decreased (*green boxed area*) or increased (*red boxed area*) in response to the PROTAC 17 treatment (*B*). *C*, chemical structure of PROTAC 17 *cis*-epimer control. *D*, Western blots showing the effect of increasing concentrations of PROTAC 17 enantiomer on LZK expression and JNK phosphorylation in response to dox-induced expression of LZK in CAL33 cells. GAPDH served as the loading control. *E*, effect of PROTAC 17 enantiomer on colony formation by the indicated cell lines. DMSO served as the vehicle control. Cells were treated for 14 days with the drug being replaced every 48 h. Plates were fixed and stained with crystal violet and visualized. DMSO, dimethyl sulfoxide; LZK, leucine zipper–bearing kinase; PROTAC, proteolysis-targeting chimera.

VHL-Adip-NHS

Di-(*N*-succinimidyl)adipate (2.97 g, 8.73 mmol, 4 equiv) was added to 24 ml of MeCN and 12 ml of DMF at room temperature. To the stirred mixture was added a suspension of VHL amine HCl salt (1.05 g, 2.18 mmol) and triethylamine (360 µl, 330 mg, 3.27 mmol, 1.5 equiv) in 3 ml of DMF. The reaction was stirred overnight and then concentrated under reduced pressure. The residue was subjected directly to flash chromatography (0–20% MeOH in DCM); the appropriate fractions were concentrated under reduced pressure to yield the final compound as a white solid (1.39 g, 20.8 mmol, 95.2% yield). ^{1}H NMR (400 MHz, $CDCl_3$) δ 8.70 (s, 1H), 7.48-7.34 (m, 5H), 6.41-6.28 (m, 1H), 5.08 (p, *J* = 7.1 Hz, 1H), 4.70 (q, *J* = 8.2 Hz, 1H), 4.57 (dd, *J* = 8.8, 2.9 Hz, 1H), 4.50 (s, 1H), 4.07 (dd, *J* = 11.3, 4.9 Hz, 1H), 3.67-3.57 (m, 2H), 2.81 (s, 4H), 2.60 (s, 1H), 2.53 (s, 3H), 2.48 (tdd, *J* = 13.0, 6.9, 3.8 Hz, 1H), 2.36-2.16 (m, 2H), 2.11-2.01 (m, 1H), 1.74 (t, *J* = 4.4 Hz, 3H), 1.63 (s, 2H), 1.47 (d, *J* = 6.9 Hz, 3H), 1.04 (d, *J* = 1.1 Hz, 9H). HRMS: Calculated for $C_{33}H_{44}N_5O_8S^+$ 670.2911, found 670.2911.

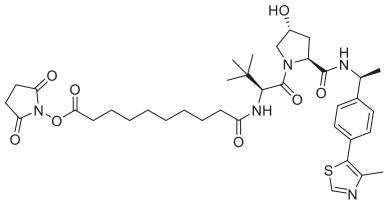

VHL-Seb-NHS

Prepared as described for VHL-Adip-NHS. 107.4 mg, 148 µmol, 71.2% yield. ^{1}H NMR (400 MHz, $CDCl_3$) δ 8.75 (s, 1H), 7.47-7.35 (m, 5H), 6.15 (d, *J* = 8.7 Hz, 1H), 5.09 (p, *J* = 7.0 Hz, 1H), 4.74 (t, *J* = 7.9 Hz, 1H), 4.56 (d, *J* = 8.7 Hz, 1H), 4.15 (dt, *J* = 11.6, 1.9 Hz, 1H), 3.59 (dd, *J* = 11.5, 3.6 Hz, 1H), 2.84 (d, *J* = 2.9 Hz, 4H), 2.60 (t, *J* = 7.4 Hz, 2H), 2.56 (s, 3H), 2.26-2.18 (m, 2H), 2.14-2.03 (m, 1H), 1.74 (p, *J* = 7.4 Hz, 2H), 1.48 (d, *J* = 6.9 Hz, 3H), 1.40 (s, 3H), 1.31 (s, 7H), 1.06 (s, 9H) HRMS: Calculated for $C_{37}H_{52}N_5O_8S^+$ 726.3537, found 726.3530.

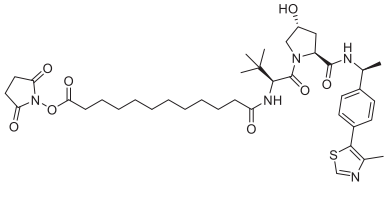

VHL-Dodec-NHS

As described for VHL-Adip-NHS. 135 mg, 179 µmol, 86.1% yield. ^{1}H NMR (400 MHz, $CDCl_3$) δ 8.76 (s, 1H), 7.49-7.35 (m, 5H), 6.12 (d, *J* = 8.6 Hz, 1H), 5.09 (p, *J* = 7.0 Hz, 1H), 4.74 (t, *J* = 7.9 Hz, 1H), 4.58-4.50 (m, 2H), 4.20-4.10 (m, 1H), 3.59 (dd, *J* = 11.4, 3.7 Hz, 1H), 2.87-2.81 (m, 4H), 2.64-2.58 (m, 2H), 2.56 (s, 3H), 2.21 (t, *J* = 7.6 Hz, 2H), 2.13-2.02 (m, 1H), 1.74 (p, *J* = 7.4 Hz, 2H), 1.59 (d, *J* = 15.7 Hz, 2H), 1.48 (d, *J* = 6.9 Hz, 3H), 1.40 (s, 3H), 1.34-1.22 (m, 11H), 1.06 (s, 9H). HRMS: Calculated for $C_{39}H_{56}N_5O_8S^+$ 754.3850, found 754.3848.

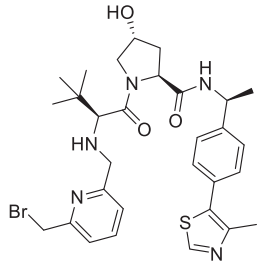

VHL-Py-CH_2Br

A solution of VHL amine HCl salt (50 mg, 104 µmol) in 1 ml of DMF was treated with 2,6-*bis*(bromomethyl)pyridine (82.6 mg, 312 µmol, 3 equiv) and sodium bicarbonate (17.5 mg, 208 µmol, 2 equiv), and the reaction was stirred overnight. The crude monoalkylated product was obtained by preparative HPLC water (0.05% TFA) with an increasing gradient of acetonitrile (0.05% TFA) followed by lyophilization to yield 11.5 mg of a white powder. The material was carried on without further purification. HRMS: Calculated for $C_{30}H_{38}BrN_5O_3S^+$ 628.1957, found 628.1954.

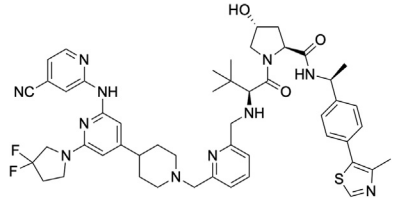

Compound 1

To a solution of VHL-Py-CH_2Br (9.7 mg, 13.4 µmol) in DMF (1 ml) was added LZK amine (6.0 mg, 15.6 µmol) and sodium bicarbonate (3.9 mg, 46.8 µmol). The reaction was stirred at ambient temperature overnight. The reaction mixture was diluted with DCM (5 ml) and water (10 ml), and the resulting layers were separated. The aqueous layer was extracted twice with DCM (2 x 5 ml). The combined organic extracts were dried over sodium sulfate, filtered, and concentrated under reduced pressure. The residue was purified by flash chromatography (0–20% MeOH in DCM) to give the desired product as a yellow solid. LC–MS: 97%% pure (254 nm). Calculated for $C_{50}H_{60}F_2N_{11}O_3^+$ 932.5, found 932.5.

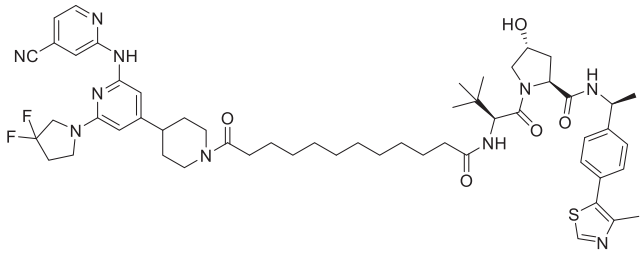

VHL-C12-LZK (2)

As described for VHL-Adip-NHS. 26.6 mg, 26 µmol, 76.9% yield. ^{1}H NMR (400 MHz, $CDCl_3$) δ 8.68 (s, 1H), 8.35 (d, *J* = 5.1 Hz, 1H), 7.46-7.34 (m, 5H), 7.05 (s, 1H), 6.16 (dt, *J* = 13.9, 6.8 Hz, 1H), 5.82 (s, 1H), 5.09 (p, *J* = 7.1 Hz, 1H), 4.82

(d, *J* = 13.1 Hz, 1H), 4.75 (t, *J* = 7.9 Hz, 1H), 4.57 (d, *J* = 8.7 Hz, 1H), 4.53 (s, 1H), 4.15 (d, *J* = 11.5 Hz, 1H), 4.00 (d, *J* = 13.6 Hz, 1H), 3.88 (t, *J* = 12.7 Hz, 2H), 3.81 (s, 2H), 3.60 (dd, *J* = 11.4, 3.6 Hz, 1H), 3.13 (t, *J* = 12.8 Hz, 1H), 2.66-2.55 (m, 2H), 2.54 (s, 3H), 2.43-2.31 (m, 2H), 2.21 (t, *J* = 7.5 Hz, 2H), 2.14-2.03 (m, 1H), 1.90 (t, *J* = 15.4 Hz, 2H), 1.63 (s, 14H), 1.48 (d, *J* = 6.9 Hz, 3H), 1.35-1.25 (m, 11H), 1.06 (s, 9H). HRMS: Calculated for $C_{55}H_{73}F_2N_{10}O_5S^+$: 1023.5454, found 1023.5452.

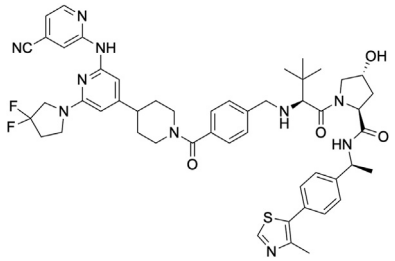

Compound 3

To a suspension of (2S,4R)-l-((S)-2-amino-3,3-dimethylbutanoyl)-4-hydroxy-*N*-((S)-l-(4-(4-methylthiazol-5-yl)phenyl) ethyl)pyrrolidine-2-carboxamide hydrochloride (22 mg, 0.046 mmol) and 4-formylbenzoic acid (9 mg, 0.06 mmol) was added sodium sulfate (55 mg) and refluxed overnight. The reaction mixture was then cooled in an ice bath and sodium borohydride (4 mg, 0.11 mmol), and the reaction was stirred until conversion was completed, as judged by LC–MS. The reaction mixture was then filtered through celite, concentrated, dissolved in DCM, and loaded onto a silica cartridge and purified by flash chromatography (0–25% methanol in DCM) to afford the free acid as a yellow solid. The aforementioned solid (22 mg, 0.038 mmol) was dissolved in DMF (2 ml) followed by the addition of 2-((6-(3,3-difluoropyrrolidin-l-yl)-4-(piperidin-4-yl)pyridin-2-20 yl)amino) isonicotinonitrile dioxalate salt (21 mg, 0.037 mmol) and NMM (26 µl, 0.23 mmol). HATU (20 mg, 0.053 mmol) was then added, and solution was stirred for 1 h, and water and DCM were added. The aqueous layer was extracted with DCM (25 ml, two times). The combined organic extracts were washed with saturated sodium bicarbonate, brine, dried over sodium sulfate, filtered, and concentrated. The crude solid was then dissolved in DCM 25 and loaded onto a silica cartridge and purified by flash chromatography (0 to 12% methanol in DCM to afford the product as a yellow solid). The product was further purified by RP-HPLC using a Waters XBridge Prep Cl8 5 µm 19 mm × 150 mm column in water (0.05% TFA) with an increasing gradient of acetonitrile (0.05% TFA). The combined fractions were lyophilized to afford the product as a fluffy yellow solid. LC–MS: 97.5% pure (254 nm). Calculated for $C_{51}H_{59}F_2N_{10}O_4S^+$ 945.4, found 945.5. LC–MS (column, water/acetonitrile [5–95% over 4 min; flow rate = 1.0 ml/min, l = 215 nm]) tR = 3.45 min (major). ^{1}H NMR (400 MHz, $CDCl_3$) δ 8.67 (s, 1H), 8.42 (s, 1H), 8.33 (d, *J* = 5.0 Hz, 1H), 7.50-7.32 (m, 8H), 7.01 (d, *J* = 4.8 Hz, 1H), 6.24 (s, 1H), 5.80 (s, 1H), 5.04 (p, *J* = 7.0 Hz, 1H), 4.88 (br s, 1H), 4.76 (br s, 1H), 4.47 (br s, 1H), 3.90-3.71 (5H), 3.42 (m, 1H),3.13 (m, 1H), 2.86 (m, 1H), 2.70 (m, 2H), 2.53 (m, 5H), 2.05-1.53 (m, 9H), 1.47 (d, *J* = 6.9 Hz, 3H), 1.03 (s, 9H). HRMS: Calculated for $C_{51}H_{59}F_2N_{10}O_4S^+$ 945.4404, found 945.4390.

Compound 4

Ellman DHP resin (730 mg, 1.01 mmol, 1.38 mmol/g) was swollen in 10 ml of 1,2-dichloroethane under argon for 1 h. To resin was added (9H-fluoren-9-yl)methyl (2S,4R)-4-hydroxy-2-(((S)-1-(4-(4-methylthiazol-5-yl)phenyl)ethyl)carbamoyl)pyrrolidine-1-carboxylate (673 mg, 1.22 mmol) and pyridinium p-toluene sulfonate (382 mg, 1.52 mmol), and the reaction mixture was stirred at 80°C overnight under argon. The resin was then washed with ample amounts of DMF, DCM, and diethyl ether. The loading was determined to be 0.315 mmol/g. The resin with attached (9H-fluoren-9-yl) methyl (2S,4R)-4-hydroxy-2-(((S)-1-(4-(4-methylthiazol-5-yl) phenyl)ethyl)carbamoyl)pyrrolidine-1-carboxylate (516 mg, 0.16 mmol) was treated with 20% piperidine in DMF for 20 min twice and washed with DMF. A solution of Fmoc-L-tert-leucine (461 mg, 1.30 mmol), HBTU (495 mg, 1.31 mmol), NMM (0.29 ml, 2.61 mmol) in DMF was added to the resin, and the reaction was agitated for 1 h. The resin was then washed repeatedly with DMF, DCM, and diethyl ether.

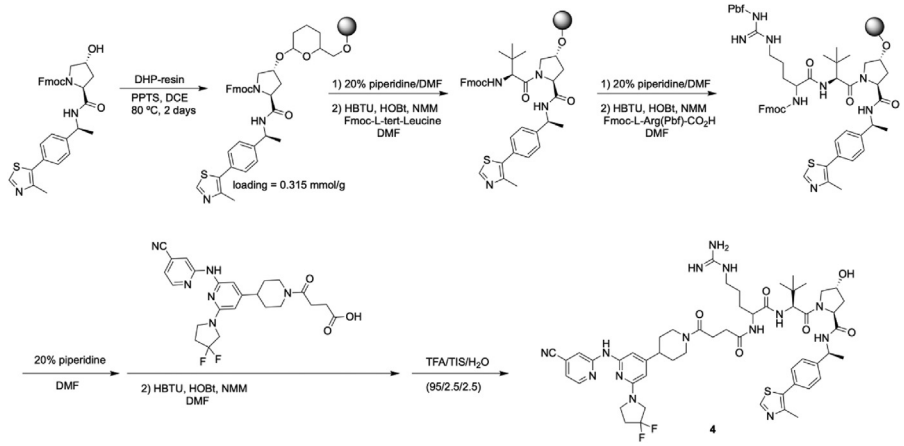

The aforementioned resin (127 mg, 0.04 mmol) was treated with 20% piperidine in DMF for 20 15 min twice and washed with DMF. A solution of Fmoc-Arg(Boc)2-OH (194 mg, 0.33 mmol), HBTU (116 mg, 0.31 mmol), NMM (72 μl, 0.64 mmol) in DMF was added to the resin, and the reaction was agitated for 1 h. The resin was then washed with DMF, DCM, and DMF again. The resin was then again treated with 20% piperidine in DMF for 20 min twice and washed with DMF, DCM, and diethyl ether. To the aforementioned resin (23 mg, 0.007 mmol) was added a solution of 4-(4-(2-((4-cyanopyridin-2-yl)amino)-6-(3,3-difluoropyrrolidin-1-yl)pyridin-4-yl)piperidin-1-yl)-4-oxobutanoic acid (27 mg, 0.056 mmol), HBTU (21 mg, 0.056 mmol), and NMM (13 μl, 0.112 mmol) in DMF, and the reaction was agitated for 1 h. The resin was then washed repeatedly with DMF, DCM, and diethyl ether. The aforementioned resin was treated with a mixture of TFA, triisopropylsilane, and water (95:2.5:2.5) for 2 h. The resin was then filtered, and the product was precipitated in anhydrous diethyl ether and centrifuged. The product was purified by RP-HPLC using a Waters XBridge Prep C18 5 μm 19 mm × 150 mm column in water (0.05% TFA) with an increasing gradient of acetonitrile (0.05% TFA). The combined fractions were lyophilized to afford the product as a yellow solid (0.5 mg, 0.47 μmoles). LC–MS: Calculated for $C_{53}H_{70}F_2N_{14}OS^{2+}$ 534.27, found 534.40.

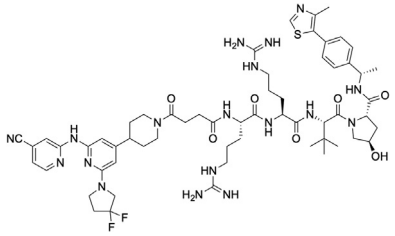

Compound 5

Prepared in a similar way to compound 4. LC–MS: 95.8% pure (254 nm). Calculated for $C_{59}H_{82}F_2N_{18}O_7S^{2+}$ 612.31, found 612.50.

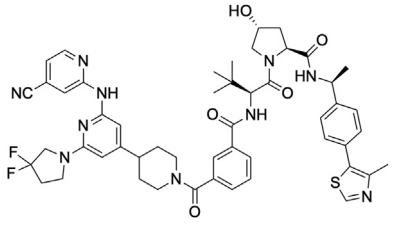

Compound 6

Prepared by general method 1

^{1}H NMR (400 MHz, DMSO-d_6) δ 9.89 (s, 1H), 8.99 (s, 1H), 8.45-8.37 (m, 3H), 8.15 (d, J = 9.0 Hz, 1H), 7.99-7.88 (m, 2H), 7.64-7.50 (m, 2H), 7.44 (d, J = 8.3 Hz, 2H), 7.38 (d, J = 8.3 Hz, 2H), 7.25-7.18 (m, 1H), 6.61 (s, 1H), 6.07 (s, 1H), 4.93 (p, J = 7.1 Hz, 1H), 4.77 (d, J = 9.0 Hz, 1H), 4.64 (br s, 1H), 4.45 (t, J = 8.1 Hz, 1H), 4.31 (m, 1H), 4.10 (m, 4H), 3.87 (t, J = 13.2 Hz, 2H), 3.73-3.61 (m, 4H), 3.16 (m, 1H), 2.87 (m, 1H), 2.77-2.68 (m, 1H), 2.64-2.52 (m, 2H), 2.44 (s, 3H) 2.08-1.98 (m, 1H), 1.66 (m, 3H), 1.37 (d, J = 7.0 Hz, 3H), 1.04 (s, 9H). HRMS: Calculated for $C_{51}H_{57}F_2N_{10}O_5S^+$ 959.4202, found 959.4190.

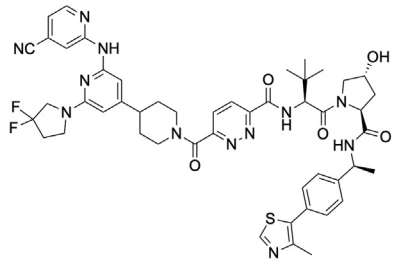

Compound 7

Prepared by general method 1

HRMS: Calculated for $C_{49}H_{55}F_2N_{10}O_5S^+$ 961.4107, found 961.4095.

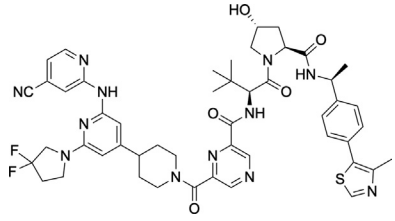

Compound 8

Prepared by general method 1

^{1}H NMR (400 MHz, DMSO-d_6) δ 9.83 (s, 1H), 8.97 (s, 1H), 8.46-8.26 (m, 3H), 7.44-7.30 (m, 4H), 7.26-7.15 (m, 1H), 6.57 (s, 1H), 6.02-5.93 (m, 1H), 5.82 (d, J = 8.9 Hz, 1H), 4.89 (q, J = 7.1 Hz, 1H), 4.50-4.33 (m, 2H), 4.32-4.26 (m, 1H), 4.10 (t, J = 12.8 Hz, 2H), 3.84 (t, J = 13.3 Hz, 2H), 3.66-3.58 (m, 52H), 2.76 (q, J = 12.2 Hz, 2H), 2.61-2.51 (m, 2H), 2.44 (s, 5H), 2.06-1.89 (m, 1H), 1.83-1.64 (m, 4H), 1.48 (dq, J = 14.3, 4.0 Hz, 2H), 1.35 (d, J = 7.0 Hz, 3H), 0.95 (s, 9H). HRMS: Calculated for $C_{49}H_{55}F_2N_{12}O_5S^+$ 961.4107, found 961.4090.

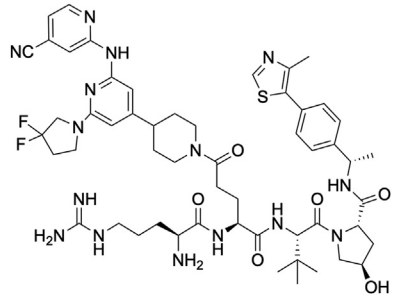

Compound 9

HATU (86 mg, 0.23 mmol) was added to a solution of Fmoc-L-glutamic acid 5-tert-butyl ester (96 mg, 0.23 mmol) and NMM (52 μl, 0.46 mmol) in DMF, and the mixture was stirred for 5 min. The activated acid was then added to a solution of (2S,4R)-l-((S)-2-amino-3,3-dimethylbutanoyl)-4-hydroxy-N-((S)-l-(4-(4-methylthiazol-5 yl)phenyl)ethyl)pyrrolidine-2-carboxamide hydrochloride (100 mg, 0.21 mmol), NMM (76 μl, 0.68 mmol) in DMF, and the reaction was stirred for 1 h at room temperature. After 1 h, water and ethyl acetate was added,

and the ethyl acetate layer was washed with water, sodium bicarbonate, and brine. The organic layer was then dried over sodium sulfate, filtered, and concentrated. The crude solid was then treated with 5 ml TFA/DCM (1:1), and the reaction was stirred for 1 h and then concentrated. The crude solid was dissolved in DMF (2 ml), and NMM was added (67 µl, 0.60 mmol), followed by HATU (76 mg, 0.23 mmol). To this solution was added a solution of 2-((6-(3,3-difluoropyrrolidin-l-yl)-4-(piperidin-4-y l)pyridin-2-yl)amino)isonicotinonitrile oxalic acid salt (98 mg, 0.23 mmol), NMM (112 µl, 1.0 mmol) in DMF (1 ml). After 1 h, water was added to the reaction mixture and extracted with ethyl acetate (3 x 20 ml). The combined organic extracts were washed with brine, dried over sodium sulfate, and concentrated. The crude solid was dissolved in DCM and loaded onto a silica cartridge and purified by flash chromatography (0 to 10% methanol in DCM to afford 69 mg of a yellow solid). This solid (0.06 mmol) was dissolved in acetonitrile (5 ml), and tetrahydrofuran (1 ml) and diethylamine was added (183 µl, 1.77 mmol) and stirred overnight. The reaction was then concentrated, redissolved in acetonitrile/water (9:1), and washed with hexane three times to afford the deprotected amine (52 mg, 0.06 mmol). To a solution of Fmoc-Arg(Boc)2-OH (14 mg; 0.02 mmol) and NMM (10 µl, 0.09 mmol) in DMF (1 ml) was added HATU (8 mg, 0.02 mmol), and the mixture was stirred for 5 min. This mixture was then added to a solution of (2S,4R)-l-((S)- 2-((S)-2-amino-5-(4-(2-((4-cyanopyridin-2-y l)amino)-6-(3,3-difluoropyrrolidin-1-yl)pyridin-4-yl)piperidin-l-yl)-5-oxopentanamido)-3,3-dimethylbutanoyl)-4-hydroxy-*N*-((S)-l-(4-(4-methylthiazol-5-yl)phenyl)ethyl)pyrrolidine-2-carboxamide (15 mg, 0.02 mmol) in DMF (1 ml), and the reaction was stirred for 1 h. Water was added to the reaction mixture and extracted with ethyl acetate (3 x 20 ml). The combined organic extracts were washed with brine, dried over sodium sulfate, and concentrated. The crude solid was dissolved in DCM and loaded onto a silica cartridge and purified by flash chromatography (0 to 20% methanol in DCM 5 to afford the product as a yellow solid). The product was further purified by RP-HPLC using a Waters XBridge Prep C18 5 µm 19 mm × 150 mm column in water (0.05% TFA) with an increasing gradient of acetonitrile (0.05% TFA). The combined fractions were lyophilized to afford the product as a yellow solid. LC–MS: (254 nm). Calculated for $C_{54}H_{72}F_2N_{15}O_6S^+$ 1096.6 found 1096.4.

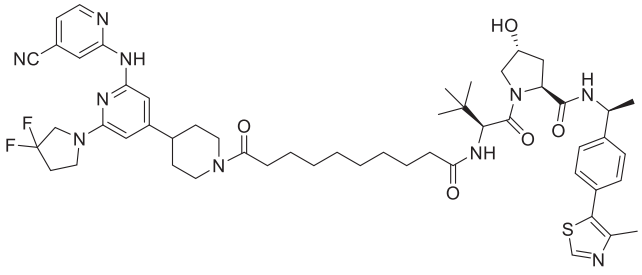

VHL-C10-LZK (10)

As described for VHL-Adip-NHS. 53.4 mg, 53.7 µmol, 95.4% yield.

^{1}H NMR (400 MHz, $CDCl_3$) δ 8.68 (s, 1H), 8.35 (d, *J* = 5.1 Hz, 1H), 7.51-7.45 (m, 1H), 7.44-7.33 (m, 4H), 7.05 (s, 1H), 6.39-6.03 (m, 1H), 5.82 (s, 1H), 5.09 (p, *J* = 7.1 Hz, 1H), 4.77 (q, *J* = 11.8 Hz, 2H), 4.59 (dd, *J* = 8.7, 4.8 Hz, 1H), 4.52 (s, 1H), 4.14 (d, *J* = 12.0 Hz, 1H), 4.00 (d, *J* = 13.7 Hz, 1H), 3.88 (t, *J* = 12.8 Hz, 2H), 3.80 (s, 2H), 3.60 (d, *J* = 11.5 Hz, 1H), 3.13 (t, *J* = 12.9 Hz, 1H), 2.66-2.54 (m, 2H), 2.53 (s, 3H), 2.36 (td, *J* = 7.3, 2.9 Hz, 2H), 2.20 (h, *J* = 6.6 Hz, 2H), 2.14-2.07 (m, 1H), 1.90 (t, *J* = 15.1 Hz, 2H), 1.64 (s, 12H), 1.48 (dd, *J* = 7.0, 2.4 Hz, 3H), 1.31 (s, 9H), 1.06 (s, 9H). HRMS: Calculated for $C_{53}H_{69}F_2N_{10}O_5S^+$: 995.5141, found 995.5141.

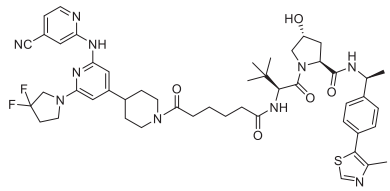

VHL-Adip-LZK (11)

VHL-Adip-NHS (25 mg, 37 µmol) and LZK amine (14.4 mg, 37 µmol) were combined in 1 ml of DMF and treated with NNMM (12.3 µL, 112 µmol, 3 equiv). After stirring overnight, the reaction was diluted with 5 ml DCM and washed with 10 ml of water. The aqueous layer was extracted with 2 x 5 ml DCM; the combined organics were dried over Na_2SO_4 and concentrated under reduced pressure. Flash chromatography (0–20% MeOH in DCM) afforded the desired product (25.8 mg, 27.5 µmol, 73.6% yield) as a yellow solid residue. ^{1}H NMR (400 MHz, $CDCl_3$) δ 8.68 (s, 1H), 8.44 (br s, 1H), 8.33 (dd, *J* = 5.2, 2.5 Hz, 1H), 7.53-7.46 (m, 1H), 7.42-7.33 (m, 4H), 7.02 (d, *J* = 4.9 Hz, 1H), 6.55 (dd, *J* = 17.5, 8.7 Hz, 1H), 6.29 (br s, 1H), 5.79 (s, 1H), 5.09 (p, *J* = 7.0 Hz, 1H), 4.82-4.73 (m, 1H), 4.62 (d, *J* = 8.8 Hz, 1H), 4.50 (s, 1H), 4.12 (d, *J* = 11.5 Hz, 1H), 3.97 (d, *J* = 13.5 Hz, 1H), 3.85 (t, *J* = 12.9 Hz, 2H), 3.76 (t, *J* = 7.1 Hz, 2H), 3.60 (dt, *J* = 11.4, 3.9 Hz, 1H), 3.11 (t, *J* = 12.9 Hz, 1H), 2.67-2.54 (m, 2H), 2.52 (s, 3H), 2.37 (q, *J* = 6.1 Hz, 1H), 2.26 (s, 2H), 2.16-2.06 (m, 1H), 1.85 (d, *J* = 14.6 Hz, 2H), 1.76-1.56 (m, 12H) 1.47 (d, *J* = 6.9 Hz, 3H), 1.22 (s, 1H), 1.06 (s, 9H). HRMS: Calculated for $C_{49}H_{61}F_2N_{10}O_5S^+$: 939.4515, found 939.4505.

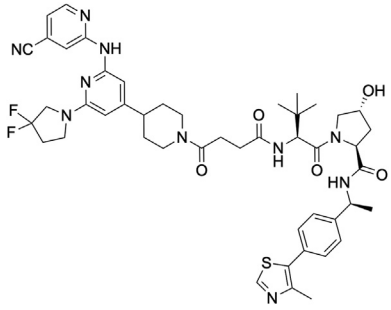

Compound 12

To a solution of 2-((6-(3,3-difluoropyrrolidin-l-yl)-4-(piperidin-4-yl)pyridin-2-yl)amino)isonicotinonitrile dioxalate salt (107 mg, 0.19 mmol) in anhydrous DMF (3 ml) was added NMM (107 µl, 0.95 mmol) and succinic anhydride (25 mg, 0.25 mmol), and the reaction was stirred overnight under argon. The crude solid was dissolved in DCM and loaded onto a silica

cartridge and purified by flash chromatography (0 to 20% methanol in DCM to afford the product as a yellow solid). ^{1}H NMR (400 MHz, CD_3OD-*d*) δ 8.41 (s, 1H), 8.35 (d, *J* = 5.1 Hz, 1H), 7.08 (d, *J* = 5.0 Hz, 1H), 6.48 (s, 1H), 6.00 (s, 1H), 4.65 (d, *J* = 13.3 Hz, 1H), 4.13 (d, *J* = 13.6 Hz, 1H), 3.87 (t, *J* = 13.1 Hz, 2H), 3.75-3.67 (m, 2H), 3.25-3.12 (m, 2H), 2.94 (m, 1H), 2.80-2.67 (m, 3H), 2.64-2.50 (m, 4H).

The acid was dissolved in DMF (2 ml), and e3 ligase VHL warhead hydrochloride (44 mg, 0.078 mmol) and anhydrous diisopropylethylamine (27 µl, 0.24 mmol) were added, and the reaction was stirred for 1 h under argon at room temperature. The reaction mixture was poured into water and extracted with DCM. The combined organic extracts were washed with brine, dried over sodium sulfate, filtered, and concentrated *in vacuo*. The crude solid was dissolved in DCM and loaded onto a silica cartridge and purified by flash chromatography (0 to 15% methanol in DCM to afford the product as a yellow solid). The product was further purified by RP-HPLC using a Waters XBridge Prep Cl8 5 µm 19 mm × 150 mm column in water (0.05% TFA) with an increasing gradient of acetonitrile (0.05% TFA). The combined fractions were lyophilized to afford the product as a fluffy yellow solid.

^{1}H NMR (400 MHz, CD_3OD) δ 8.86 (s, 1H), 8.54-8.42 (m, 2H), 8.33 (d, *J* = 5.2 Hz, 1H), 7.98 (m, 2H), 7.42 (m, 4H), 7.04 (d, *J* = 5.1 Hz, 1H), 6.48 (s, 1H), 5.96 (s, 1H), 5.01 (p, *J* = 6.7 Hz, 1H), 4.69-4.51 (m, 3H), 4.43 (m, 1H), 4.10 (d, *J* = 13.9 Hz, 1H), 3.94-3.79 (m, 3H), 3.78-3.66 (m, 3H), 3.17 (m, 1H), 2.79-2.49 (m, 8H), 2.20 (m, 1H), 2.00-1.82 (m, 4H), 1.76-1.53 (m, 3H), 1.50 (d, *J* = 7.0 Hz, 3H), 1.05 (s, 9H). HRMS: Calculated for $C_{47}H_{57}F_2N_{10}O_5S^+$ 911.4197, found 911.4189.

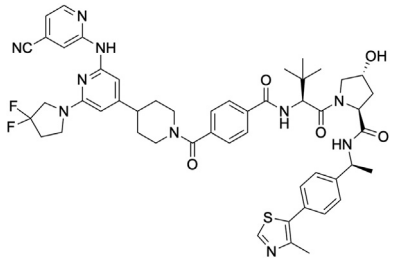

Compound 13

Prepared by general method 1

^{1}H NMR (400 MHz, $CDCl_3$) δ 8.67 (s, 1H), 8.42 (s, 1H), 8.33 (d, *J* = 5.0 Hz, 1H), 7.50-7.32 (m, 8H), 7.01 (d, *J* = 4.8 Hz, 1H), 6.24 (s, 1H), 5.80 (s, 1H), 5.10 (p, *J* = 7.0 Hz, 1H), 4.92-4.80 (m, 2H), 4.71 (t, *J* = 7.9 Hz, 1H), 4.54, (s, 1H), 4.13 (d, *J* = 11.4 Hz, 1H), 3.85 (t, *J* = 12.9 Hz, 2H), 3.78-3.66 (m, 3H), 3.09 (m, 1H), 2.86 (m, 1H), 2.69 (m, 1H), 2.57-2.42 (m, 5H), 2.10-1.88 (m, 5H), 1.76 (m, 2H), 1.49 (d, *J* = 7.0 Hz, 3H), 1.12 (s, 9H). HRMS: Calculated for $C_{51}H_{57}F_2N_{10}O_5S^+$ 959.4197, found 959.4196.

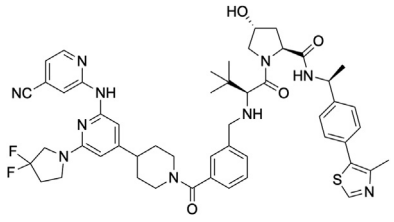

Compound 14

Prepared by the same method as compound **3**

^{1}H NMR (400 MHz, DMSO-d_6) δ 9.85 (s, 1H), 9.19 (br s, 1H), 8.97 (s, 1H), 8.65 (br s, 1H), 8.54 (d, J = 7.8 Hz, 1H), 8.42-8.38 (m, 2H), 7.60-7.56 (m, 2H), 7.53-7.47 (m, 2H), 7.42 (d, *J* = 8.3 Hz, 2H), 7.36 (d, *J* = 8.3 Hz, 2H), 7.20 (dd, *J* = 5.0, 1.4 Hz, 1H), 6.60 (s, 1H), 6.00 (s, 1H), 4.91 (p, *J* = 7.1 Hz, 1H), 4.82-4.57 (m, 3H), 4.53 (t, *J* = 8.2 Hz, 1H), 4.28 (s, 1H), 4.16 (d, *J* = 13.3 Hz, 1H), 3.94 (d, *J* = 13.3 Hz, 1H), 3.84 (t, *J* = 13.2 Hz, 2H), 3.73 (br s, 1H), 3.64 (t, *J* = 7.2 Hz, 2H), 3.43-3.32 (m, 2H), 3.17 (m, 1H), 2.87 (m, 1H), 2.73 (m, 1H), 2.61-2.51 (m, 2H), 2.43 (s, 3H), 2.09 (m, 1H), 1.88 (m, 1H), 1.77 (m, 1H), 1.73-1.50 (m, 3H), 1.37 (d, *J* = 7.0 Hz, 1H), 1.03 (s, 9H).

HRMS: Calculated for $C_{51}H_{59}F_2N_{10}O_4S^+$ 945.4410, found 945.4402.

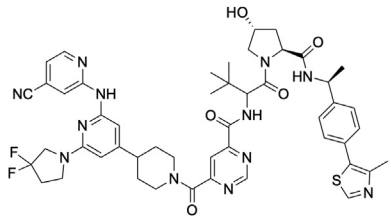

Compound 15

Prepared by general method 1

^{1}H NMR (400 MHz, DMSO-d_6) δ 9.90 (s, 1H), 9.42 (d, *J* = 1.4 Hz, 1H), 8.99 (s, 1H), 8.56 (dd, *J* = 9.6, 3.2 Hz, 1H), 8.48 (dd, *J* = 7.8, 1.9 Hz, 1H), 8.45-8.41 (m, 2H), 8.13 (t, *J* = 1.1 Hz, 1H), 7.48-7.40 (m, 2H), 7.38 (d, *J* = 8.3 Hz, 2H), 7.26-7.18 (m, 2H), 7.05 (d, *J* = 51.1 Hz, 1H), 6.60 (s, 1H), 6.04 (s, 1H), 4.93 (p, *J* = 7.1 Hz, 1H), 4.72 (d, *J* = 9.6 Hz, 1H), 4.62 (d, *J* = 13.0 Hz, 1H), 4.46 (td, *J* = 8.3, 3.0 Hz, 1H), 4.30 (d, *J* = 4.0 Hz, 1H), 3.87 (t, *J* = 13.3 Hz, 2H), 3.70-3.59 (m, 5H), 3.27-3.14 (m, 1H), 2.99-2.89 (m, 1H), 2.73 (d, *J* = 11.6 Hz, 1H), 2.58 (dq, *J* = 14.2, 7.1 Hz, 2H), 2.46 (s, 3H), 2.07 (dd, *J* = 12.9, 7.9 Hz, 1H), 1.90 (d, *J* = 12.7 Hz, 1H), 1.80 (d, *J* = 13.0 Hz, 0H), 1.69 (s, 2H), 1.53 (t, *J* = 7.6 Hz, 1H), 1.39 (d, *J* = 7.0 Hz, 3H), 1.02 (s, 9H). HRMS: Calculated for $C_{49}H_{55}F_2N_{10}O_5S^+$ 961.4107, found 961.4099.

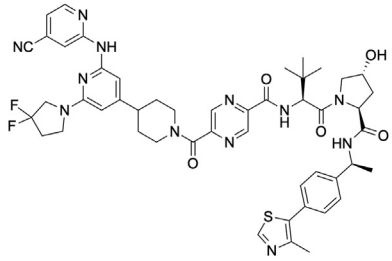

Compound 16

Prepared by general method 1

^{1}H NMR (400 MHz, DMSO-d_6)δ 9.94 (s, 1H), 9.22-9.18 (m, 1H), 9.00-8.93 (m, 2H), 8.46 (dd, *J* = 7.7, 2.0 Hz, 1H), 8.43-8.36 (m, 3H), 7.46-7.30 (m, 4H), 7.20 (dd, *J* = 5.1, 1.4 Hz, 1H), 6.58 (s, 1H), 6.03 (s, 1H), 4.91 (p, *J* = 7.1 Hz, 1H), 4.80-4.69 (m, 5H), 4.65 (d, *J* = 13.1 Hz, 1H), 4.60-4.40 (m, 18H), 4.29 (dq, *J* = 5.0, 2.5 Hz, 1H), 3.86 (t, *J* = 13.2 Hz, 2H), 3.74 (d, *J* = 13.1 Hz, 1H), 3.69-3.57 (m, 4H), 3.25-3.14 (m, 1H), 2.93 (td, *J* = 13.0, 2.8 Hz, 1H), 2.75 (ddt, *J* = 11.9, 7.4, 3.8 Hz, 1H), 2.56 (dq, *J* = 14.4, 7.2 Hz, 2H), 2.44 (s, 3H),

2.11-2.01 (m, 1H), 1.96-1.87 (m, 1H), 1.83-1.60 (m, 4H), 1.37 (d, J = 7.0 Hz, 3H), 1.00 (s, 9H). ^{13}C NMR (126 MHz, $CDCl_3$) δ 171.30, 169.69, 164.62, 162.62, 157.32, 156.20, 154.54, 152.56, 151.92, 150.48, 149.15, 148.59, 143.70, 143.58, 143.20, 142.38, 131.70, 131.01, 129.67, 126.55, 121.45, 117.35, 117.04, 114.16, 98.63, 98.58, 97.28, 77.42, 77.16, 76.91, 70.31, 60.52, 58.70, 57.85, 56.91, 54.51, 54.25, 53.99, 49.05, 47.80, 44.68, 43.25, 42.69, 36.00, 35.76, 34.15, 33.11, 32.12, 26.66, 22.35, 21.16, 16.21, 14.31. HRMS: Calculated for $C_{49}H_{55}F_2N_{12}O_5S^+$ 961.4107, found 961.4097.

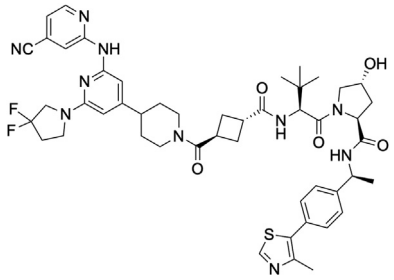

Compound 17

Prepared by general method 1

^{1}H NMR (500 MHz, DMSO-d_6) δ 9.96 (s, 1H), 8.99 (s, 1H), 8.44-8.35 (m, 3H), 7.74 (t, J = 7.8 Hz, 1H), 7.43 (d, J = 8.0 Hz, 2H), 7.38 (d, J = 8.0 Hz, 2H), 7.26-7.19 (m, 1H), 7.09 (d, J = 51.1 Hz, 1H), 6.56 (s, 1H), 6.02 (s, 1H), 4.91 (p, J = 7.1 Hz, 1H), 3.86 (t, J = 13.1 Hz, 2H), 3.71-3.60 (m, 5H), 3.33 (p, J = 7.9 Hz, 1H), 3.15 (p, J = 7.8 Hz, 1H), 3.03 (t, J = 12.8 Hz, 1H), 2.60 (dtt, J = 36.5, 15.2, 8.1 Hz, 4H), 2.45 (s, 2H), 2.37-2.21 (m, 2H), 2.02 (td, J = 9.0, 4.5 Hz, 1H), 1.79 (ddd, J = 21.8, 10.9, 6.9 Hz, 3H), 1.49 (dtd, J = 25.0, 12.3, 4.6 Hz, 2H), 1.37 (d, J = 7.0 Hz, 3H), 0.94 (s, 9H). ^{13}C NMR (126 MHz, DMSO) δ 174.25, 171.78, 171.71, 170.66, 169.53, 158.68, 158.39, 158.10, 157.96, 155.07, 154.61, 152.23, 151.54, 149.08, 147.72, 144.70, 131.19, 130.47, 129.69, 128.85, 128.51, 126.56, 126.41, 126.24, 120.26, 117.39, 116.33, 113.82, 98.78, 97.17, 68.82, 58.60, 56.60, 56.29, 53.84, 53.59, 53.34, 47.73, 44.76, 44.32, 41.93, 41.55, 40.11, 40.02, 39.94, 39.85, 39.78, 39.69, 39.61, 39.52, 39.44, 39.35, 39.19, 39.02, 37.77, 35.30, 34.19, 33.36, 33.24, 33.17, 32.99, 32.51, 31.84, 27.46, 26.45, 22.44, 15.97. HRMS: Calculated for $C_{49}H_{59}F_2N_{10}O_5S^+$ 937.4353, found 937.4357. LC–MS (column, water/acetonitrile (5–95% over 4 min; flow rate = 1.0 ml/min, l = 254 nm) tR = 3.72 min (major).

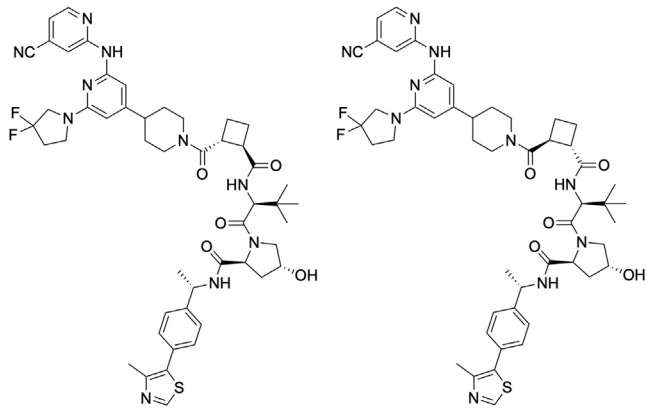

Compound 18/19

Prepared by general method 1

Isomer were separated by RP-HPLC. Isomer 1: ^{1}H NMR (500 MHz, DMSO-d_6) δ 9.89 (s, 1H), 8.98 (d, J = 1.5 Hz, 1H), 8.44-8.36 (m, 3H), 7.47-7.39 (m, 2H), 7.37 (dd, J = 8.4, 1.7 Hz, 2H), 7.22 (dd, J = 5.1, 1.4 Hz, 1H), 6.57 (d, J = 5.4 Hz, 1H), 5.97 (d, J = 44.3 Hz, 1H), 4.91 (p, J = 7.4 Hz, 1H), 4.45 (ddt, J = 22.8, 14.8, 8.4 Hz, 3H), 4.28 (q, J = 3.5 Hz, 1H), 4.11 (s, 18H), 3.85 (td, J = 13.2, 7.8 Hz, 2H), 3.69-3.56 (m, 4H), 3.52-3.33 (m, 2H), 3.03 (q, J = 13.6 Hz, 1H), 2.71-2.50 (m, 4H), 2.45 (s, 3H), 2.16-2.05 (m, 1H), 2.07 (s, 2H), 2.01 (t, J = 7.9 Hz, 1H), 1.97-1.87 (m, 2H), 1.78 (ddt, J = 12.5, 8.6, 4.2 Hz, 3H), 1.46 (s, 1H), 1.37 (d, J = 7.0, Hz, 3H), 0.91 (m, 9H) (rotamers). LC–MS: Calculated for $C_{49}H_{59}F_2N_{10}O_5S^+$ 937.44, found 937.50. Isomer 2: ^{1}H NMR (500 MHz, DMSO) δ 9.91 (s, 1H), 8.99 (d, J = 1.6 Hz, 1H), 8.44-8.36 (m, 2H), 7.81 (dd, J = 11.8, 9.3 Hz, 1H), 7.46-7.24 (m, 4H), 7.21 (ddd, J = 8.4, 5.5, 2.8 Hz, 1H), 6.56 (d, J = 3.9 Hz, 1H), 6.03 (d, J = 16.2 Hz, 1H), 4.89 (dp, J = 21.6, 7.1 Hz, 1H), 4.55-4.50 (m, 1H), 4.50-4.40 (m, 1H), 4.31 (s, 12H), 4.28 (t, J = 3.8 Hz, 1H), 3.88 (d, J = 13.1 Hz, 1H), 3.85-3.74 (m, 1H), 3.69-3.40 (m, 5H), 3.05-2.92 (m, 1H), 2.66-2.51 (m, 3H), 2.49-2.43 (m, 3H) (rotamers), 2.13-2.02 (m, 1H), 1.99 (dd, J = 9.8, 6.5 Hz, 1H), 1.99-1.83 (m, 1H), 1.78 (ddd, J = 14.3, 9.4, 6.0 Hz, 3H), 1.46 (ddd, J = 25.2, 12.9, 8.0 Hz, 2H), 1.38 (d, J = 7.0 Hz, 1H) (rotamer), 1.31 (d, J = 7.0 Hz, 1H) (rotamer), 0.93 (s, 9H). LC–MS: Calculated for $C_{49}H_{59}F_2N_{10}O_5S^+$ 937.44, found 937.50.

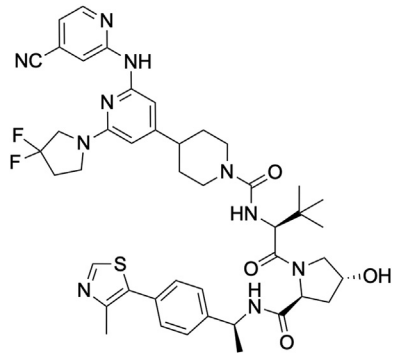

Compound 20

To a solution of 2-((6-(3,3-difluoropyrrolidin-1-yl)-4-(piperidin-4-yl)pyridin-2-yl)amino)isonicotinonitrile dioxalate salt in anhydrous DCM (3 ml) was added triphosgene (37 mg, 0.079 mmol) under argon. Anhydrous diisopropylethylamine (54 µl, 0.48 mmol) was added. After 30 min was added (2S,4R)-1-((S)-2-amino-3,3-dimethylbutanoyl)-4-hydroxy-*N*-((S)-1-(4-(4-methylthiazol-5-yl)phenyl)ethyl)pyrrolidine-2-carboxamide hydrochloride (44 mg, 0.078 mmol) and anhydrous diisopropylethylamine (27 µl, 0.24 mmol), and the reaction was stirred for 1 h under argon at room temperature. The reaction mixture was poured into water and extracted with DCM. The combined organic extracts were washed with brine, dried over sodium sulfate, filtered, and concentrated *in vacuo*. The crude solid was dissolved in DCM and loaded onto a silica cartridge

and purified by flash chromatography (0 to 15% methanol in DCM to afford the product as a yellow solid).

The product was further purified by RP-HPLC using a Waters XBridge Prep C18 5 μm 19 mm × 150 mm column in water (0.05% TFA) with an increasing gradient of acetonitrile (0.05% TFA). The combined fractions were lyophilized to afford the product as a fluffy yellow solid. ^{1}H NMR (400 MHz, DMSO-d_6) δ 9.83 (s, 1H), 8.97 (s, 1H), 8.46-8.26 (m, 3H), 7.44-7.30 (m, 4H), 7.26-7.15 (m, 1H), 6.57 (s, 1H), 6.02-5.93 (m, 1H), 5.82 (d, *J* = 8.9 Hz, 1H), 4.89 (q, *J* = 7.1 Hz, 1H), 4.50-4.33 (m, 2H), 4.32-4.26 (m, 1H), 4.10 (t, *J* = 12.8 Hz, 2H), 3.84 (t, *J* = 13.3 Hz, 2H), 3.66-3.58 (m, 52H), 2.76 (q, *J* = 12.2 Hz, 2H), 2.61-2.51 (m, 2H), 2.44 (s, 5H), 2.06-1.89 (m, 1H), 1.83-1.64 (m, 4H), 1.48 (dq, *J* = 14.3, 4.0 Hz, 2H), 1.35 (d, *J* = 7.0 Hz, 3H), 0.95 (s, 9H). LC–MS: 99.1% pure (254 nm). Calculated for $C_{44}H_{53}F_2N_{10}O_4S^+$ 855.4, found 855.3.

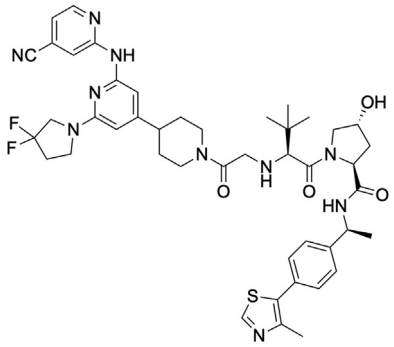

Compound 21

To a solution of chloroacetic acid (14 mg, 0.15 mmol, 1.7 eq) and NMM (0.02 ml, 0.18 mmol, 2 eq) in DMF (1 ml) was added HATU (38 mg, 0.1 mmol, 1.1 eq). After 5 min, this solution was added to a solution of of 2-((6-(3,3-5 difluoropyrrolidin-1-yl)-4-(piperidin-4-y1)pyridin-2-y1)amino)isonicotinonitrile dioxalate salt (50 mg, 0.09 mmol, 1 eq) and NMM (0.05 ml, 0.45 mmol, 5 eq) in anhydrous DMF (1 ml). The reaction was stirred for 1 h after which water was added. The reaction mixture was partitioned between water and DCM, and the aqueous layer was extracted with DCM twice. The combined organic extracts were washed with saturated $NaHCO_3$ and brine. The organic layer was then dried over sodium sulfate, filtered, and concentrated *in vacuo*. The crude solid was dissolved in DCM and loaded onto a silica cartridge and purified by flash chromatography (0 to 10% methanol in DCM to afford the 2-chloroacetyl intermediate as a yellow solid). This intermediate (21 mg, 0.05 mmol, 1 eq) was dissolved in acetonitrile (3 ml). To this solution was added (2S,4R)-1-((S)-2-amino-3,3-dimethylbutanoyl)-4-hydroxy-*N*-((S)-1-(4-(4-methylthiazol-5-yl) phenyl)ethyl)pyrrolidine-2-carboxamidehydrochloride (22 mg, 0.05 mmol, 1 eq), potassium carbonate (31 mg, 0.22 mmol, 5 eq), and potassium iodide (4 mg, 0.02 mmol, 0.5 eq). The reaction was then stirred at 80°C for 7 h. The reaction mixture was cooled to room temperature, filtered, and concentrated. The crude was partitioned between water and DCM. The organic layer was washed with brine, dried over sodium sulfate, filtered, and concentrated *in vacuo*. The crude solid was dissolved in DCM and loaded onto a silica cartridge and purified by flash chromatography (0 to 10% methanol in DCM to afford the product as a yellow solid). The product was further purified by RP-HPLC using a Waters XBridge Prep C18 5 μm 19 mm × 150 mm column in water (0.05% TFA) with an increasing gradient of acetonitrile (0.05% TFA). The combined 25 fractions were lyophilized to afford the product as a fluffy yellow solid. LC–MS: 94.0% pure (254 nm). Calculated for $C_{45}H_{55}F_2N_{10}O_4S^+$ 869.4, found 869.4.

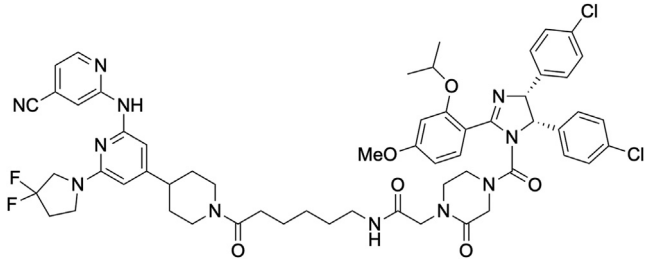

Compound 22

LC–MS: Calculated for $C_{58}H_{64}Cl_2F_2N_{11}O_6^+$ 1118.4, found 1118.0.

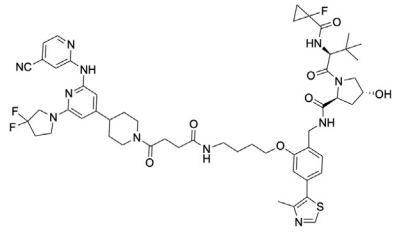

Compound 23

To a solution of 4-(4-(2-((4-cyanopyridin-2-yl)amino)-6-(3,3-difluoropyrrolidin-1-yl)pyridin-4-yl)piperidin-1-yl)-4-oxobutanoic acid (13 mg, 0.027 mmol) and (2*S*,4*R*)-*N*-(2-(4-aminobutoxy)-4-(4-methylthiazol-5-yl)benzyl)-1-((*S*)-2-(1-fluorocyclopropane-1-carboxamido)-3,3-dimethylbutanoyl)-4-hydroxypyrrolidine-2-carboxamide dihydrochloride (12 mg, 0.018 mmol) in DMF (1.5 ml) was added NMM (12 μl, 0.107 mmol) and HATU (10 mg, 0.026 mmol). The reaction was stirred for 1 h after which water and ethyl acetate were added, and the mixture was stirred for 10 min. The layers were then partitioned, and the aqueous layer was extracted with ethyl acetate twice, and the combined organic extracts were washed with brine, dried over sodium sulfate, filtered, and concentrated under reduced pressure.

The residue was purified by RP-HPLC (water/acetonitrile [0.05% TFA]) to give the desired product as a yellow solid. ^{1}H NMR (400 MHz, DMSO-d_6) δ 9.93 (s, 1H), 8.96 (s, 1H), 8.49 (t, *J* = 6.0 Hz, 1H), 8.41 (d, *J* = 5.1 Hz, 1H), 8.37 (s, 1H), 7.84 (t, *J* = 5.6 Hz, 1H), 7.39 (d, *J* = 7.8 Hz, 1H), 7.27 (dd, *J* = 9.3, 2.9 Hz, 1H), 7.21 (dd, *J* = 5.1, 1.4 Hz, 1H), 6.98 (d, *J* = 1.6 Hz, 1H), 6.93 (dd, *J* = 7.8, 1.6 Hz, 1H), 6.55 (s, 1H), 6.00 (s, 1H), 4.67 (d, *J* = 7.4 Hz, 0H), 4.62-4.56 (m, 1H), 4.50 (t, *J* = 8.2 Hz, 2H), 4.46-4.39 (m, 0H), 4.36-4.28 (m, 1H), 4.26 (d, *J* = 6.2 Hz, 1H), 4.20 (d, *J* = 5.7 Hz, 1H), 4.16 (d, *J* = 5.6 Hz, 0H), 4.03 (t, *J* = 6.3 Hz, 2H), 3.97 (d, *J* = 13.5 Hz, 1H), 3.85 (t, *J* = 13.2 Hz,

2H), 3.68-3.51 (m, 4H), 3.08 (dd, *J* = 13.7, 7.4 Hz, 3H), 2.73-2.50 (m, 1H), 2.44 (s, 3H), 2.34-2.24 (m, 2H), 2.16-2.00 (m, 1H), 1.90 (ddd, *J* = 13.0, 8.9, 4.5 Hz, 1H), 1.74 (dq, *J* = 11.3, 4.6 Hz, 4H), 1.62-1.51 (m, 3H), 1.45-1.28 (m, 2H), 1.23-1.12 (m, 2H), 0.93 (s, 9H). HRMS: Calculated for $C_{54}H_{67}F_3N_{11}O_7S^+$ 1070.4898, found 1070.4901.

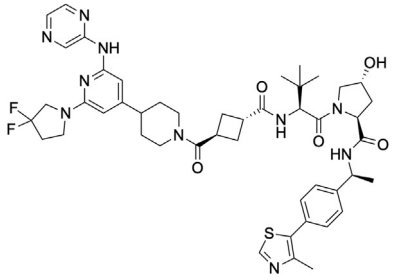

Compound 24

Prepared by general method 1

LC–MS: Calculated for C47H59F2N10O5S+ 913.4, found 913.2.

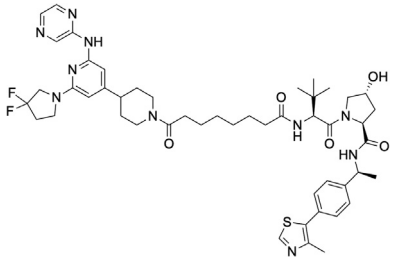

Compound 25

Prepared by general method 1

LC–MS: Calculated for $C_{49}H_{65}F_2N_{10}O_5S^+$ 943.5, found 943.2.

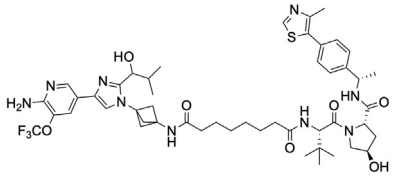

Compound 26

^{1}H NMR (400 MHz, DMSO-d_6) δ 8.97 (s, lH), 8.63 (s, lH), 8.43 (d, J = 2.0 Hz, lH), 8.35 (d, J = 7.8 Hz, lH), 8.07 (s, lH), 8.00 (t, J = 1.8 Hz, lH), 7.76 (d, J = 9.3 Hz, lH), 7.51- 7.23 (m, 4H), 4.90 (t, J = 7.2 Hz, lH), 4.68 (d, J = 7.1 Hz, lH), 4.50 (d, J = 9.3 Hz, lH), 4.40 (t, J = 8.0 Hz, lH), 4.26 (s, lH), 3.59 (d, J = 4.5 Hz, 2H), 2.75 - 2.56 (m, 6H), 2.43 (s, 3H), 2.23 (dt, J = 14.7, 15 7.7 Hz, lH), 2.15 -1.95 (m, 4H), 1.78 (ddd, J = 12.9, 8.5, 4.7 Hz, lH), 1.46 (s, 6H), 1.36 (d, J = 7.0 Hz, 3H), 1.23 (d, J = 7.3 Hz, 1H), 1.00 (d, J = 6.6 Hz, 3H), 0.92 (s, 9H), 0.82 (d, J = 6.7 Hz, 3H). ^{13}C NMR (101 MHz, DMSO) 8173.54, 172.47, 171.06, 170.06, 153.44, 151.95, 151.92, 150.20, 148.18, 145.10, 131.56, 130.24, 130.13, 129.27, 126.83, 126.71, 122.22, 119.65, 118.11, 116.97, 115.18, 110.00, 69.20, 59.00, 56.79, 56.70, 56.39, 49.02, 48.14, 44.02, 38.19, 35.83, 35.64, 20 35.34, 33.93, 28.92, 28.90, 26.90, 25.78, 25.31, 22.86, 19.14, 18.00, 16.41. LC–MS: Calculated for $C_{49}H_{65}F_3N_9O_7S^+$ 980.47, found 980.200.

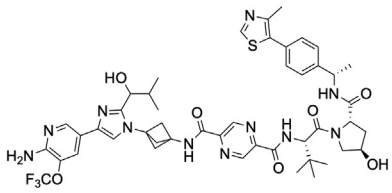

Compound 27

Prepared by general method 1

LC–MS: Calculated for $C_{47}H_{55}F_3N_{11}O_7S^+$ 974.4, found 974.2.

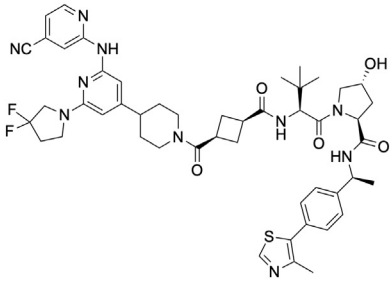

Compound 28 (17 cis*-epimer)*

Prepared by general method 1

^{1}H NMR (400 MHz, DMSO-d_6) δ 9.90 (s, 1H), 8.97 (s, 1H), 8.43-8.31 (m, 3H), 7.70 (d, *J* = 9.2 Hz, 1H), 7.42 (d, *J* = 8.3 Hz, 2H), 7.36 (d, *J* = 8.3 Hz, 2H), 7.21 (dddd, *J* = 17.3, 9.1, 5.1, 1.4 Hz, 1H), 6.54 (s, 1H), 6.00 (s, 1H), 4.90 (p, *J* = 7.0 Hz, 1H), 4.52-4.36 (m, 3H), 4.27 (s, 2H), 3.83 (q, *J* = 13.4 Hz, 3H), 3.68-3.54 (m, 4H), 3.25-3.07 (m, 2H), 3.01 (t, *J* = 12.6 Hz, 1H), 2.69-2.49 (m, 4H), 2.44 (s, 3H), 2.40-2.12 (m, 2H), 2.00 (ddd, *J* = 10.7, 7.7, 2.6 Hz, 1H), 1.77 (ddd, *J* = 12.9, 8.7, 3.6 Hz, 3H), 1.49-1.39 (m, 2H), 1.35 (d, *J* = 7.0 Hz, 3H), 0.91 (s, 9H). HRMS: Calculated for $C_{49}H_{59}F_2N_{10}O_5S^+$ 937.4353, found 937.4352.

Protein lysate preparation and immunoblot analysis

Cells were plated in 35-mm plates for 24 h in 10% FBS media and treated with dox for 48 h. Media were then removed and replenished with additional dox and treatment with specific PROTAC using 5% FBS media for 24 h. Following treatment, cells were washed with ice-cold PBS without Ca and Mg (Quality Biological) and then lysed on ice with radioimmunoprecipitation assay buffer (50 mM NaCl, 1.0% IGEPAL CA-630, 0.5% sodium deoxycholate, 0.1% SDS, 50 mM Tris, pH 8.0) (Sigma–Aldrich) supplemented with protease inhibitor tablet (Sigma–Aldrich) and phosphatase inhibitor cocktails 2 and 3 (Sigma–Aldrich) for 10 min. Cell lysis was followed by centrifugation at 15,000 rpm for 10 min at 4°C. Protein concentrations of the cell lysates were then determined using 660 nm PierceProtein Assay Reagent (ThermoFisher Scientific). Cellular proteins were denatured, subjected to SDS-PAGE, transferred to polyvinylidene difluoride membranes (Bio-Rad), and blocked for 2 h using 5% bovine serum albumin (BSA) in

PBS and 0.1% Tween-20. Polyvinylidene difluoride membranes were then incubated with specific antibodies (as listed in Table S1) overnight in 5% BSA–PBS with Tween-20 at 4°C, followed by 1 h incubation with the appropriate horseradish peroxidase–conjugated secondary antibodies (as listed in Table S1). Protein signals were detected using Pierce ECL Western Blotting Substrate (ThermoFisher Scientific).

Colony-formation assays

Colony-formation assays stained with crystal violet were used to measure cell growth and survival after treatment with varying concentrations of lead PROTAC. Cells were plated in triplicate in 12-well plates for 24 h. Following this, drug treatments were added using 10% FBS media and replaced every 48 h over a period of 14 days. Cells were then washed with PBS and fixed in ice-cold methanol for 10 min. Following this, cells were stained with 0.5% Crystal Violet Solution Gram Stain (Fisher) in 25% methanol for 30 min. Imaging was done using a ChemiDoc MP Imaging System (Bio-Rad). Quantification was achieved by dissolving crystal violet stain in 33% acetic acid for 20 min with shaking and measuring absorbance at 595 nm using iMark Microplate Absorbance Reader (Bio-Rad). Graphs display percent colony formation relative to DMSO-treated control sample.

In vitro *kinase assay*

An *in vitro* kinase assay was used to identify the binding affinity of our lead LZK-targeting PROTAC to the target kinase, LZK. KINOMEscan is based on a competition binding assay that quantitatively measures the ability of a compound to compete with an immobilized, active site–directed ligand. Briefly, kinase-tagged T7 phage strains were prepared in an *Escherichia coli* host derived from the BL21 strain. The lysates were centrifuged and filtered to remove cell debris. The remaining kinases were produced in human embryonic kidney-293 cells and subsequently tagged with DNA for quantitative PCR detection. Streptavidin-coated magnetic beads were treated with biotinylated small-molecule ligands for 30 min at room temperature to generate affinity resins for kinase assays. The liganded beads were blocked with excess biotin and washed with blocking buffer (SeaBlock [Pierce], 1% BSA, 0.05% Tween-20, and 1 mM DTT) to remove unbound ligand and to reduce nonspecific binding. Binding reactions were assembled by combining kinases, liganded affinity beads, and test compounds in 1x binding buffer (20% SeaBlock, 0.17x PBS, 0.05% Tween-20, and 6 mM DTT). Test compounds were prepared as 111X stocks in 100% DMSO. K_ds were determined using an 11-point threefold compound dilution series with three DMSO control points. The assay plates were incubated at room temperature with shaking for 1 h, and the affinity beads were washed with wash buffer (1x PBS and 0.05% Tween-20). The beads were then resuspended in elution buffer (1x PBS, 0.05% Tween-20, 0.5 μM nonbiotinylated affinity ligand) and incubated at room temperature with shaking for 30 min. The kinase concentration in the eluates was measured by quantitative PCR.

Mass spectrometric analysis

Cells were seeded on a 6-well plate at a density of 150,000 cells/well. The next day, cells were treated with dox for 24 h, followed by treatment with 500 nM PROTAC 19 or DMSO as a control. After 24 h, cells were lysed in urea lysis buffer (8 M urea in 100 mM Tris, pH 8.5) and subjected to sample preparation and LC–MS analysis.

Samples were subjected to chloroform–methanol precipitation, and the resulting protein pellets were washed twice with methanol. The protein pellets were air-dried for ∼10 min and resuspended in 100 mM Hepes (pH 8) by vigorous vortexing and sonication. Proteins were then reduced and alkylated with 10 mM Tris(2-carboxyethyl)phosphine hydrochloride/40 mM chloroacetamide and digested with trypsin in a 1:50 (w/w) enzyme-to-protein ratio at 37°C overnight. Digestion was terminated by the addition of TFA to a 1% final concentration. The resulting peptides were labeled using an on-column tandem mass tag (TMT) labeling protocol. TMT-labeled samples were compiled into a single TMT sample and concentrated using a SpeedVac concentrator. Peptides in the compiled sample were separated into eight fractions by off-line basic reversed phase using the Pierce High pH Reversed-Phase Peptide Fractionation Kit (Thermo Fisher Scientific).

Prior to the LC–MS measurement, the peptide fractions were resuspended in 0.1% TFA and 2% acetonitrile in water. Chromatographic separation was performed on an Easy-Spray Acclaim PepMap column (50 cm length × 75 μm inner diameter; Thermo Fisher Scientific) at 55°C by applying 120 min acetonitrile gradients in 0.1% aqueous formic acid at a flow rate of 300 nl/min. An UltiMate 3000 nano-LC system was coupled to a Q Exactive HF-X mass spectrometer *via* an easy-spray source (all Thermo Fisher Scientific). The Q Exactive HF-X was operated in TMT mode with survey scans acquired at a resolution of 60,000 at *m/z* 200. Up to 15 of the most abundant isotope patterns with charges 2 to 5 from the survey scan were selected with an isolation window of 0.7 *m/z* and fragmented by higher-energy collision dissociation with normalized collision energies of 32, whereas the dynamic exclusion was set to 35 s. The maximum ion injection times for the survey scan and dual MS (MS/MS) scans (acquired with a resolution of 45,000 at *m/z* 200) were 50 and 120 ms, respectively. The ion target value for MS was set to 3e6 and for MS/MS was set to 1e5, and the minimum automatic gain control target was set to 1e3.

The data were processed with MaxQuant, version 1.6.17.0 (Max-Plank Institute of Biochemistry) (17) and the peptides were identified from the MS/MS spectra searched against UniProt human reference proteome (UP000005640) using the built-in Andromeda search engine. Reporter ion MS2-based quantification was applied with reporter mass tolerance = 0.003 Da and minimum reporter precursor ion fraction = 0.75. Cysteine carbamidomethylation was set as a fixed modification and methionine oxidation, glutamine/asparagine deamination, as well as protein N-terminal acetylation were set as variable modifications. For *in silico* digests of the reference proteome, cleavages of arginine or lysine followed by

any amino acid were allowed (trypsin/P), and up to two missed cleavages were allowed. The false discovery rate was set to 0.01 for peptides, proteins, and sites. A match between runs was enabled. Other parameters were used as preset in the software. Unique and razor peptides were used for quantification enabling protein grouping (razor peptides are the peptides uniquely assigned to protein groups and not to individual proteins). Reporter intensity–corrected values for protein groups were loaded into Perseus, version 1.6.10.0 (Constellation Software Inc.) (18). Standard filtering steps were applied to clean up each dataset: reverse (matched to decoy database), only identified by site, and potential contaminant (from a list of commonly occurring contaminants included in MaxQuant) protein groups were removed. Reporter intensity–corrected values were Log2 transformed. Protein groups with all values and at least two unique + razor peptides were kept. Reporter intensity values were then normalized by median subtraction within TMT channels. Student's *t* tests were performed on these values for groups of samples constituting a given dataset. The abundance change thresholds of Log2 fold change ≥|1.0| and the significance threshold of –Log10 *p* value ≥2.0 were applied to deliver protein groups with levels deemed reproducibly decreased or increased between the sample groups investigated. The data are available *via* ProteomeXchange Consortium (19) *via* the PRIDE partner repository (20) with the dataset identifier PXD057778.

Parallel artificial membrane permeability assay

PAMPA was utilized to measure passive, transcellular permeation in an *in vitro* model by Cyprotex. Compounds are treated with a Lucifer Yellow integrity marker and tested at 10 μM for their ability to pass through a hexadecane in hexane (5% v/v) membrane over a period of 5 h. To determine the level of diffusion across the membrane, compounds are analyzed using LC–MS/MS quantification. Compounds are tested in four replicates and standardized to identify the mean permeability.

Time-lapse microscopy

Cells were plated in 96-well plates with full growth media more than 24 h before imaging, such that the density would remain subconfluent until the end of the imaging period. Time-lapse imaging was performed in 290 μl of full growth media. Images were taken in cyan fluorescent protein and yellow fluorescent protein channels every 12 min on a Nikon Ti2-E inverted microscope (Nikon) with a 20 × 0.45 numerical aperture objective. Total light exposure time was kept under 600 ms for each time point. Cells were imaged in a humidified, 37°C chamber at 5% CO_2.

Image analysis

All image analyses were performed with custom MATLAB scripts as previously described (21). In brief, optical illumination bias was empirically derived by sampling background areas across all wells in an imaging session and was subsequently used to flatten all images. This enabled measurement and subtraction of a global background for each image. Cells were segmented for their nuclei on the basis of H2B-mTurquoise. CDK2 activity was calculated by measuring the nuclear and cytoplasmic fluorescence of the DHB-mVenus protein. Cells were segmented for their cytoplasmic regions by spatially approximating a ring with an inner radius of 2 μm outside the nuclear mask and an outer radius with a maximum of 10 μm outside the nuclear mask. Regions within 10 μm of another nucleus were excluded. Cytoplasmic DHB-mVenus was calculated as the median intensity within the cytoplasmic ring, excluding pixel intensities indistinguishable from background.

Mitosis events were automatically identified using H2B-mTurquoise and called at anaphase when one cell split into two daughter cells, each with approximately 45 to 55% of the size of the mother cell. Cells were considered to have been arrested in the G_2 phase if a second mitosis was not detected for more than 30 h after the first mitosis. After drug treatment, cells were categorized by their CDK2 activity 2 h after anaphase. Cells with high CDK2 activity (defined as greater than 0.6) were considered to have immediately reentered the cell cycle, cells with transiently low CDK2 activity (defined as less than 0.6 2 h after anaphase but rising to greater than 0.6 within the viewing time) were considered to have entered into a transient G_0 state before eventually reentering the cell cycle, and cells with low CDK2 activity (defined as less than 0.6 within the viewing time) were to have entered a prolonged G_0 state (22).

Quantification and statistical analysis

All samples represent biological replicates. Data are presented as the mean with error bars shown on graphs representing ±SD. Two-tailed Student's *t* test was used to assess significance of differences between groups for colony-formation assay with Welch correction when variance between groups was significantly different as analyzed with *F* test. Values of $p < 0.05$ were considered as significantly different.

Data availability

Data from MS are deposited in a publicly accessible repository and available *via* ProteomeXchange Consortium (44) *via* the PRIDE partner repository (45) with the dataset identifier PXD057778.

Supporting information—This article contains supporting information.

Author contributions—M. K., A. L. F., R. E. S., and J. F. B. conceptualization; M. K. and J. F. B. methodology; K. L. B., M. R. R., A. L. F., C. C. W., K. N., K. K., R. S., and A. M. validation; M. K., K. L. B., E. L., M. R. R., A. L. F., C.C.W., K.N., K.K., R.S., A.M., and R.E.S. investigation; M. K., K. L. B., and E.L. data curation; M. K., E. L., R. E. S., and J. F. B. writing–original draft; M. K., E. L., and J. F. B. writing–review & editing; R. S., A. M., R. E. S., and J. F. B. supervision; M. K., A. L. F., and J. F. B. project administration; R. E. S. and J. F. B. funding acquisition.

Funding and additional information—This research was supported by the National Cancer Institute, grant number ZIA BC 011691. In addition, this research was supported by the National Institutes of Health Intramural Research Program through a National Cancer Institute FLEX award to J.B. The MS experiment was supported by National Science Center, Poland (2021/42/E/NZ5/00227) award to A.A.M. The content of this publication neither does necessarily reflect the views or policies of the Department of Health and Human Services nor does mention of trade names, commercial products, or organizations imply endorsement by the US government.

Conflict of interest—The authors declare a patent filed for the National Cancer Institute with inventors J. F. B., R. E. S, C. C. W., A. L. F., K. L. B., and K. N. for the development of novel PROTACs to target LZK in HNSCC to promote tumor regression. All other authors declare that they have no conflicts of interest with the contents of this article.

Abbreviations—The abbreviations used are: BSA, bovine serum albumin; DCM, dichloromethane; DMF, dimethylformamide; DMSO, dimethyl sulfoxide; dox, doxycycline; FBS, fetal bovine serum; HATU, O-(7-azabenzotriazol-1-yl)-N,N,N',N'-tetramethyluronium hexafluorophosphate; HNSCC, head and neck squamous cell carcinoma; HRMS, high-resolution mass spectrometry; JNK, c-Jun N-terminal kinase; LZK, leucine zipper–bearing kinase; MS, mass spectrometry; NMM, N-methylmorpholine; PAMPA, parallel artificial membrane permeability assay; pen–strep, penicillin–streptomycin; POI, protein of interest; PROTAC, proteolysis-targeting chimera; RP-HPLC, reverse-phase HPLC; TMT, tandem mass tag.

References

1. Sakuma, H., Ikeda, A., Oka, S., Kozutsumi, Y., Zanetta, J. P., and Kawasaki, T. (1997) Molecular cloning and functional expression of a cDNA encoding a new member of mixed lineage protein kinase from human brain. *J. Biol. Chem.* **272**, 28622–28629
2. Jin, Y., and Zheng, B. (2019) Multitasking: dual leucine zipper-bearing kinases in neuronal development and stress management. *Annu. Rev. Cell Dev. Biol.* **35**, 501–521
3. Masaki, M., Ikeda, A., Shiraki, E., Oka, S., and Kawasaki, T. (2003) Mixed lineage kinase LZK and antioxidant protein-1 activate NF-κB synergistically. *Eur. J. Biochem.* **270**, 76–83
4. Ikeda, A., Masaki, M., Kozutsumi, Y., Oka, S., and Kawasaki, T. (2001) Identification and characterization of functional domains in a mixed lineage kinase LZK. *FEBS Lett.* **488**, 190–195
5. Chen, M., Geoffroy, C. G., Meves, J. M., Narang, A., Li, Y., Nguyen, M. T., *et al.* (2018) Leucine zipper-bearing kinase is a critical regulator of astrocyte reactivity in the adult mammalian CNS. *Cell Rep.* **22**, 3587–3597
6. Edwards, Z. C., Trotter, E. W., Torres-Ayuso, P., Chapman, P., Wood, H. M., Nyswaner, K., *et al.* (2017) Survival of head and neck cancer cells relies upon LZK kinase-mediated stabilization of mutant p53. *Cancer Res.* **77**, 4961–4972
7. Craig, R. A., 2nd, Fox, B. M., Hu, C., Lexa, K. W., Osipov, M., Thottumkara, A. P., *et al.* (2022) Discovery of potent and selective dual leucine zipper kinase/leucine zipper-bearing kinase inhibitors with neuroprotective properties in in vitro and in vivo models of amyotrophic lateral sclerosis. *J. Med. Chem.* **65**, 16290–16312
8. Comprehensive genomic characterization of head and neck squamous cell carcinomas. *Nature* **517**, (2015), 576–582
9. Funk, A. L., Katerji, M., Afifi, M., Nyswaner, K., Woodroofe, C. C., Edwards, Z. C., *et al.* (2025) Targeting c-MYC and gain-of-function p53 through inhibition or degradation of the kinase LZK suppresses the growth of HNSCC tumors. *Sci. Signal.* **18**, eado2857
10. Liu, Z., Hu, M., Yang, Y., Du, C., Zhou, H., Liu, C., *et al.* (2022) An overview of PROTACs: a promising drug discovery paradigm. *Mol. Biomed.* **3**, 46
11. Sun, X., Gao, H., Yang, Y., He, M., Wu, Y., Song, Y., *et al.* (2019) PROTACs: great opportunities for academia and industry. *Signal Transduct. Targeted Ther.* **4**, 64
12. Patel, S., Cohen, F., Dean, B. J., De La Torre, K., Deshmukh, G., Estrada, A. A., *et al.* (2015) Discovery of dual leucine zipper kinase (DLK, MAP3K12) inhibitors with activity in neurodegeneration models. *J. Med. Chem.* **58**, 401–418
13. Diehl, C. J., and Ciulli, A. (2022) Discovery of small molecule ligands for the von Hippel-Lindau (VHL) E3 ligase and their use as inhibitors and PROTAC degraders. *Chem. Soc. Rev.* **51**, 8216–8257
14. Ikeda, A., Hasegawa, K., Masaki, M., Moriguchi, T., Nishida, E., Kozutsumi, Y., *et al.* (2001) Mixed lineage kinase LZK forms a functional signaling complex with JIP-1, a scaffold protein of the c-Jun NH(2)-terminal kinase pathway. *J. Biochem.* **130**, 773–781
15. Brognard, J. F., Swenson, R. E., Funk, A. L., Hitko, C. W., Nyswaner, K. M., Lindberg, E., *et al.*, National Center for Biotechnology Information (2024) *Lzk-targeting degraders and methods of use*. National Library of Medicine (US), Bethesda (MD). PubChem Patent Summary for US-2024190838-A1
16. Sindhu, S. K., and Bauman, J. E. (2019) Current concepts in chemotherapy for head and neck cancer. *Oral Maxillofac. Surg. Clin. North Am.* **31**, 145–154
17. Tyanova, S., Temu, T., and Cox, J. (2016) The MaxQuant computational platform for mass spectrometry-based shotgun proteomics. *Nat. Protoc.* **11**, 2301–2319
18. Tyanova, S., Temu, T., Sinitcyn, P., Carlson, A., Hein, M. Y., Geiger, T., *et al.* (2016) The Perseus computational platform for comprehensive analysis of (prote)omics data. *Nat. Methods* **13**, 731–740
19. Deutsch, E. W., Csordas, A., Sun, Z., Jarnuczak, A., Perez-Riverol, Y., Ternent, T., *et al.* (2017) The ProteomeXchange consortium in 2017: supporting the cultural change in proteomics public data deposition. *Nucleic Acids Res.* **45**, D1100–D1106
20. Perez-Riverol, Y., Bai, J., Bandla, C., García-Seisdedos, D., Hewapathirana, S., Kamatchinathan, S., *et al.* (2022) The PRIDE database resources in 2022: a hub for mass spectrometry-based proteomics evidences. *Nucleic Acids Res.* **50**, D543–D552
21. Cappell, S. D., Chung, M., Jaimovich, A., Spencer, S. L., and Meyer, T. (2016) Irreversible APC^{Cdh1} underlies the point of No return for cell-cycle entry. *Cell* **166**, 167–180
22. Arora, M., Moser, J., Phadke, H., Basha, A. A., and Spencer, S. L. (2017) Endogenous replication stress in mother cells leads to quiescence of daughter cells. *Cell Rep.* **19**, 1351–1364